CLASSIFICATION CANCELLED

CONFIDENTIAL RM No. L6J09

RESTRICTED

CLASSIFICATION CANCELLED

NACA

CLASSIFICATION CHANGED

To Unclassified
By authority of NASA Memo dtd [illegible] /s/ by [illegible]
Changed by [illegible] Date [illegible]

RESEARCH MEMORANDUM

CLASSIFICATION CANCELLED

HIGH-SPEED WIND-TUNNEL TESTS OF A $\frac{1}{16}$-SCALE MODEL

OF THE D-558 RESEARCH AIRPLANE

LIFT AND DRAG CHARACTERISTICS OF THE D-558-1

AND VARIOUS WING AND TAIL CONFIGURATIONS

By

John B. Wright and Donald L. Loving

Langley Memorial Aeronautical Laboratory
Langley Field, Va.

CLASSIFICATION CANCELLED

CLASSIFIED DOCUMENT

This document contains classified information affecting the National Defense of the United States within the meaning of the Espionage Act, USC 50:31 and 32. Its transmission or the revelation of its contents in any manner to an unauthorized person is prohibited by law.
Information so classified may be imparted only to persons in the military and naval services of the United States, appropriate civilian officers and employees of the Federal Government who have a legitimate interest therein, and to United States citizens of known loyalty and discretion who of necessity must be informed thereof.

NATIONAL ADVISORY COMMITTEE
FOR AERONAUTICS
WASHINGTON

RESTRICTED

CLASSIFICATION CANCELLED

NACA RM No. L6J09

NATIONAL ADVISORY COMMITTEE FOR AERONAUTICS

RESEARCH MEMORANDUM

HIGH-SPEED WIND-TUNNEL TESTS OF A $\frac{1}{16}$-SCALE MODEL OF THE D-558 RESEARCH AIRPLANE LIFT AND DRAG CHARACTERISTICS OF THE D-558-1 AND VARIOUS WING AND TAIL CONFIGURATIONS

By John B. Wright and Donald L. Loving

SUMMARY

Tests were made in the Langley 8-foot high-speed tunnel to investigate the aerodynamic characteristics of the D-558-1 airplane and various wing and tail configurations on the D-558-1 fuselage. The various wing and tail configurations were tested to determine the aerodynamic effects of aspect ratio and sweep for suitable use on the second phase of the D-558 project (D-558-2). The tests were conducted through a speed range from a Mach number of 0.40 to approximately 0.94. This part of the investigation includes the lift and drag results available for the configurations tested to this date.

The D-558-1 results indicated that the lift force break would occur at a Mach number of 0.85 with some reduction in lift at speeds above this Mach number. Tests indicated that the airplane will have satisfactory lift and drag characteristics up to and including its design Mach number of 0.85.

The 35° swept-back, 35° swept-forward, and low-aspect-ratio (2.0) wing configurations all showed pronounced improvements in maintaining lift throughout the Mach number range tested and in increasing the critical speeds above the D-558-1 value to critical Mach numbers on the order of 0.9. Insofar as lift and drag characteristics are concerned level flight at speeds approaching the velocity of sound appears practical if swept or low-aspect-ratio configurations similar to those tested are used.

INTRODUCTION

In order to obtain level-flight data through the transonic speed range, a series of high-speed research airplanes is being procured for

the NACA through the cooperation of the Bureau of Aeronautics, Navy Department. The Douglas Aircraft Corporation has undertaken the construction of these airplanes and they are designated collectively by Douglas Aircraft Corporation as the D-558 project. Because of the unavailability of satisfactory airplane power plants at the start of the project, the project was divided into two phases. Phase I is an airplane (D-558-1) powered solely by a turbo-jet unit and designed to fly at a maximum level flight Mach number of 0.85, while Phase II (D-558-2) is to be a rocket plus turbo-jet powered airplane to extend the maximum speed in level flight to a Mach number greater than 1.0.

The final design of the D-558-1 was frozen in July 1945 and it was thought that wind-tunnel tests at high Mach numbers of a model of D-558-1 would be desirable as a guide for the pilot during test flights and to insure against any catastrophic events. As more and more confirmatory test data (both American and German) became available on the effects of variation in wing plan form, it was decided to test various wing and tail configurations for possible use on the Phase II airplane since the design was in the nebulous state.

Accordingly, tests were made in the Langley 8-foot high-speed tunnel on a $\frac{1}{16}$-scale model of the D-558-1 with no nose-inlet flow. Tests were also made on various wing and tail configurations for possible use on the D-558-2 airplane. This report, presents those lift and drag results for which complete tare corrected data are available.

SYMBOLS

V	free-stream velocity, feet per second
ρ	free-stream density, slugs per cubic foot
q	free-stream dynamic pressure, pounds per square foot, $\left(\frac{1}{2}\rho V^2\right)$
a	free-stream velocity of sound, feet per second
M	free-stream Mach number, $\left(\frac{V}{a}\right)$
L	lift, pounds
D	drag, pounds

S_W wing area, square feet (See table II.)

C_L lift coefficient, $\left(\frac{L}{qS_W}\right)$

C_D drag coefficient $\left(\frac{D}{qS_W}\right)$

α angle of attack (fuselage center line), degrees

i_t angle of incidence of horizontal tail relative to fuselage center line, degrees

δ_e elevator angle relative to horizontal tail, degrees

$\frac{L}{D}$ lift-drag ratio

$dC_L/d\alpha$ lift-curve slope

A aspect ratio

Λ sweepback angle of the wing

APPARATUS

The D-558 investigation was conducted in the Langley 8-foot high-speed tunnel which is a single-return closed-throat type. The maximum Mach number was 0.94 for this investigation.

Model support system.- A sting-strut support system designed for these tests is shown in figure 1. The sting is a continuation of the rear of the model fuselage with provision for angle-of-attack change near the tail. The sting is connected to a vertical strut which is mounted on the tunnel-balance ring. The strut and part of the sting are shielded from the air stream by means of the fairings shown. A liner to constrict the flow was installed in the throat of the tunnel, figure 1, in order to obtain the highest possible test Mach numbers at the model location for this sting-strut system.

Model.- A $\frac{1}{16}$-scale model of the D-558-1 airplane, figure 2, was constructed according to Douglas drawing number 5,254,672, with the exception of the fin, wing-fillet, and nose inlet. The fin was built from specifications furnished by the Douglas Aircraft Corporation. On this fin, the horizontal tail is held 11-inches (full scale) higher than the upper tail position on the reference drawing. The nose inlet was faired out to form a solid nose shape thus eliminating inlet and internal flow. The various parts of the D-558-1 will be

referred to as "original" whenever used in conjunction with other proposed parts.

A wing-fuselage fillet was designed by the NACA because information on the fillet developed by Douglas Aircraft Corporation and GALCIT was not available at the start of these tests. The NACA fillet is characterized in general by having a flat surface along the root chord and is compared with the Douglas fillet in figure 3. During the course of the D-558-1 model investigation, the Douglas fillet was tested. The lift and drag results proved to be so nearly the same as to be considered identical to NACA fillet results. Therefore, even though the data presented for the D-558-1 model are with the NACA fillet, they are also representative of the Douglas fillet.

Additional wings, tails, and a fin, designed for possible use on the second airplane of the D-558 series, were made to be tested on the fuselage of the D-558-1 model. These plan forms were selected to obtain high force-break Mach numbers on the basis of information in such references as 1 to 6. The parts included a 35° swept-back wing, tail, and fin; a 35° swept-forward wing; and an unswept wing and tail with an aspect ratio of 2.0. The component parts having an aspect ratio of 2.0 will be called "low aspect ratio."

Table I is presented as an aid in determining the various configurations. The geometry and dimensions of the wings and tails tested are given in table II. As will be noted, the wing section, area, taper ratio, dihedral, and location of the 25-percent mean aerodynamic chord along the fuselage are the same for the four wings tested. The swept-back, swept-forward, and original wings also had the same aspect ratio, span, and mean aerodynamic chord. The swept wings were designed by rotating the 50-percent-chord line 35°, and shaping the tips parallel to the fuselage center line. The section profiles were perpendicular to the 50-percent-chord line, hence the percent thickness of the swept wings in the stream direction is smaller than the percent thickness perpendicular to the 50-percent-chord line or that of the unswept wings in the stream direction. Drawings of the various configurations are shown in figures 4, 5, and 6.

METHODS

Determination of tare forces.- Auxiliary arms in the vertical plane of the fuselage were used to support the model for the determination of the tare forces. These tare arms are shown as dashed lines in figure 1. The forward part of each arm was a 6-percent airfoil swept back 30° to minimize interference effects and prevent attainment of shock-wave disturbances. The remaining parts of the tare arms were

thin plates extended back to the strut. Guy wires from the wing tips were used on all tare runs so that the system would be rigid when no sting was used. Two tare setups were required to evaluate the tare forces and these are shown, with the method used to obtain corrected model data, in figure 7. In tare-run B, a short afterbody was used at the tail of the fuselage because the sting was not used on this setup. As a result, the corrected data are for the model with the afterbody. Since the model tests did not simulate nose-inlet flow or the exhausting jet at the rear of the fuselage, these data give results without these effects. All drag data in this report are tare-corrected model data. The lift tare was found to be negligible so no corrections were applied.

Accuracy.- The lift data are presented out to a Mach number of about 0.94, where choking occurs at the strut. The data are unaffected by choke phenomena as the strut was well aft of the model and pressure measurements indicated no irregularities in the velocity field in the model region. No corrections for tunnel-wall interference have been applied to these data. At a Mach number of 0.94, the calculated wall correction, to the Mach number and dynamic pressure according to references 7 to 10, would be about 2.9 percent at large angles of attack and about 1.9 percent at small angles. At a Mach number of 0.9 the tunnel-wall correction would be about 1.5 percent for large angles of attack and 1.0 percent for small angles.

Corrections to the angle of attack arise from two sources and are algebraically additive: (1) from tunnel wall and, (2) from deflection of the model under load. The angle-of-attack tunnel-wall correction in degrees at a Mach number of 0.94, would be 9 percent of the lift coefficient.

Incomplete measurements have indicated that aerodynamic loads caused a bending of the sting approximately in proportion to the lift load involved. The maximum average angle of attack increase was approximately 0.7° at lift coefficients on the order of 0.70 at a Mach number of 0.94. However, at small angles of attack throughout the speed range tested the error becomes insignificant, and it is in this region of small lift coefficients that most of the information is desired.

RESULTS

Table I is a list of all the configurations tested with the figure number and data presented for each configuration. The average Reynolds numbers based on the mean aerodynamic chord of the wings for this test are given in figure 8 as a function of Mach number.

Figures 9 through 12 show the variation of lift coefficient with Mach number for various angles of attack for all the configurations tested. A comparison of the variation of lift coefficient with Mach number for several complete configurations and the wing of reference 1 (aspect ratio = 9) is presented in figure 13. The results of figure 13 are for angles of attack corresponding to two values of low-speed lift coefficient which were selected to represent a high-speed and a gradual pull-out condition. The slopes of the lift curves $dC_L/d\alpha$ for several complete configurations are shown in figure 14. The slopes for each Mach number were found at the two values of lift coefficient required for level flight at sea level and 35,000 feet altitude as shown in figure 15. The wing loading was assumed to be 53.9 pounds per square foot, the design loading of the D-558-1 at the start of a high-speed flight run. The angle of attack for a lift coefficient of zero is presented in figure 16 for various configurations.

The variation of drag coefficient with Mach number is presented in figure 17 for several wing and tail configurations. These configurations include the D-558-1 with and without the horizontal tail; the model with the original wing, low-aspect-ratio tail, and original fin; and the complete swept-back model. Figure 18 presents the drag results in polar form C_L versus C_D for the complete original (D-558-1) and the complete swept-back configurations. From the polar plots, the drag coefficients at lift coefficients of 0.1 and 0.4 were obtained and are shown in figure 19 as a function of Mach number. Data from reference 1 are also included for comparison.

The variation of lift-drag ratio with lift coefficient is shown in figure 20 at two Mach numbers for the D-558-1 and the complete swept-back configuration. Figure 21 presents the maximum lift-drag ratio as a function of Mach number.

DISCUSSION

Lift

D-558-1.- The results of lift measurements on the D-558-1 model (fig. 9) indicate a large improvement in the high-speed lift characteristics in comparison with more conventional aircraft. At a level-flight lift coefficient of 0.1, for example, the lift coefficient begins to drop at a Mach number of 0.85. As this is the design Mach number, the important requirement of having no force break occur up to the design speed is satisfied. Following the force break, the lift decreases to a Mach number of 0.91 and then increases almost to its pre-force break value at the highest test Mach number, 0.94.

The magnitude of this lift loss is about 50 percent smaller than the loss with the wing of reference 1. The wing of reference 1 had the same thickness and a 0.1 greater design lift coefficient than the D-558-1 wing, but the aspect ratio was 9.0 as compared to 4.2 for the D-558-1. Therefore, the increase in force-break Mach number as well as the lessening in the severity of the lift loss after force break is principally the result of lower wing aspect ratio. Reference 2 results indicate similar improvements for the same amount of reduction in aspect ratio.

The slope of the lift curve $dC_L/d\alpha$ of the D-558-1 at low speeds shows good agreement with aspect-ratio theory of reference 7. However, with increase in Mach number the aspect-ratio theory gives slightly lower values of $dC_L/d\alpha$. (See fig. 14.) The test results indicate the increase in the slope with Mach number is slower and the reduction following the force break is smaller than for the wing of reference 1. These variations with Mach number as well as the delay in the increase of the angle of zero lift are due principally to the reduced aspect ratio.

Those longitudinal-stability difficulties which arise from losses in wing lift at supercritical speeds will be delayed and reduced with the D-558-1 because of the lessening of the lift loss following force break. Some adverse effects, however, will probably take place beyond a Mach number of 0.85 due to the amount of lift loss which does occur. The effects of the various tails tested on the high-speed lift characteristics are in general negligible. (See fig. 9.)

Wing and tail plan-form modifications.- The 35° swept-back, 35° swept-forward, and low-aspect-ratio (2.0) configurations all have lift breaks at Mach numbers on the order of 0.91 at lift coefficients of 0.1. (See figs. 10 to 12.) The changes in lift following the breaks are less severe and the losses, particularly at high angles, are much smaller than for the D-558-1. As indicated by these data, the D-558-2 should not experience lift difficulties in level flight to a Mach number of 0.91 if any of the wing and tail configurations shown in figures 4, 5, and 6 are used.

The slopes of the lift curves shown in figure 14 do not have severe force breaks through a Mach number of 0.9. The swept-back and swept-forward configurations have values of $dC_L/d\alpha$ similar to that of the D-558-1 at low speeds. The low-aspect-ratio wing configuration has a value of the slope of the lift curve of 0.052 at low speeds or 68 percent of that of the D-558-1. This low-speed slope is in close agreement with low-aspect-ratio theory at low Mach numbers. The rise in $dC_L/d\alpha$ with Mach number is very gradual for the low-aspect-ratio model. The angle of attack for a lift

coefficient of zero for all the modifications is about -1.7° with a small rise in the angle starting at a Mach number of 0.90. (See fig. 16.)

Thus, it has been shown that by changes in wing plan form from that used on the D-558-1 the high-speed lift characteristics have been greatly improved. Therefore, it is reasonable to expect that the pitching-moment, which is dependent on the wing retaining its lift, probably will show also some improvement through a Mach number of 0.9 when low-aspect-ratio or swept wings are used.

Drag

D-558-1.- The drag coefficient begins to rise at a Mach number of 0.82 at a lift coefficient of 0.1. (See fig. 19.) This force-break Mach number is higher than that of any airplane model with an unswept wing which previously has been tested. In the study of the effects of aspect ratio on the increase of the Mach number at which the drag rises, reference 2, it is indicated that a reduction in aspect ratio for a wing alone not only increases the value of Mach number at the force break but also reduces the rate of drag rise following the force break. In the tests of the D-558-1 the rate of drag increase is about the same as with conventional aircraft. The effects of tail plan forms tested on the high-speed drag characteristics of the D-558-1 are negligible as seen from figure 17.

Wing and tail plan-form modification.- The 35° swept-back wing and tail configuration has a greatly delayed drag force break in comparison with the D-558-1. (See fig. 19.) At a lift coefficient of 0.1, the force-break Mach number is just discernible at the highest Mach number tested, 0.91. At higher lift coefficients, 0.4 for example, the drag force break occurs within the test speed range, and the rate of the drag rise after force break appears to be smaller than for the D-558-1. The increase in force break, at a lift coefficient of 0.1, is about 55 percent of the increase predicted by the use of the $\frac{1}{\cos \Lambda}$ theoretical correction (Λ is the sweepback angle of the wing). The fuselage and fuselage interference effects are the probable cause for the increase not checking the theory. However, the delay obtained is in agreement with other test results. Reference 5 shows an increase in force-break Mach number gained by 35° of sweep (25-percent chord) of the same magnitude as attained in these tests. In both cases, the aspect ratio was held constant for the unswept and swept wings.

The swept-back configuration, therefore, has vastly improved drag characteristics in the highest test Mach number range. At

Mach numbers between 0.91 and 1.0 (the design speed for the D-558-2), some rise in drag coefficient will probably occur, but it is not known from these tests how severe this rise will be.

Lift-Drag Ratio

A sizeable reduction in lift-drag ratio for the D-558-1 is indicated at the design lift coefficient (on the order of 0.1) from low speeds up to the design Mach number of 0.85. (See fig. 20.) The L/D value is approximately 40 percent less at a Mach number of 0.85 than the value of 4.3 at a Mach number of 0.40. At a Mach number of 0.90 the L/D value is about 70 percent less than at a Mach number of 0.40. Thus a large thrust power is indicated for flight at Mach numbers of 0.85 and above. The lift-drag ratio for the swept-back configuration at any lift coefficient remains about the same for all Mach numbers through the highest speed tested. A much higher Mach number will thus be possible with these configurations than for the D-558-1 from the standpoint of power required.

The maximum lift-drag ratio for the D-558-1, figure 21, is about 12 up to a Mach number of 0.75. At this point the value begins decreasing to 6.5 at a Mach number of 0.85. The maximum lift-drag ratio for the swept-back configuration is the same value as the D-558-1 at low speeds. However, in this case the value is maintained out to a Mach number of 0.82 before a small reduction occurs to a value of 10 at a Mach number of 0.9.

Concluding Remarks

On the basis of Langley 8-foot high-speed tunnel tests of the D-558-1 model through a Mach number of 0.94 for lift and 0.91 for drag, the following conclusions have been made:

1. The airplane will have satisfactory lift and drag characteristics through its design Mach number of 0.85.

2. The lift force break occurs at a Mach number of 0.85 at a lift coefficient of 0.1, with relatively small loss following the force break. At a Mach number of 0.94, the lift coefficient is almost at its pre-force break value.

3. The drag force break at a lift coefficient of 0.1 occurs at a Mach number of 0.82.

4. The lift-drag ratio L/D at a lift coefficient of 0.1 is 40 percent less at the design Mach number of 0.85 than at a Mach number of 0.40.

5. The comparatively high force-break Mach numbers result principally from the use of a wing whose aspect ratio (4.2) is lower than those in current use.

Tests of various wing and tail plan forms intended for possible use on the D-558-2 airplane have yielded the following:

1. The 35° swept-back configuration appears to have no pronounced lift or drag force break up to a Mach number of 0.91 at a lift coefficient of 0.1.

2. The 35° swept-back configuration indicates no sizeable change in L/D for any lift coefficients throughout the Mach number range tested.

3. The 35° swept-forward wing has an effect, similar to the swept-back wing, of increasing the lift force-break Mach number to about 0.91 and reducing the amount of lift loss following. No drag results are available for this configuration at this time.

4. The effect of using a low-aspect-ratio (2.0), no-sweep configuration was to increase the lift force-break Mach number to about 0.91 with a small loss thereafter. No drag results are available for this configuration at this time.

5. Insofar as lift and drag characteristics are concerned level flight at speeds approaching the velocity of sound appears practical if swept or low-aspect-ratio configurations similar to those tested are used.

Langley Memorial Aeronautical Laboratory
National Advisory Committee for Aeronautics
Langley Field, Va.

John B. Wright

John B. Wright
Aeronautical Engineer

Donald L. Loving

Donald L. Loving
Aeronautical Engineer

Approved: L. J. Turner Jr.

for John Stack
Chief of Compressibility Research Division

cjb

REFERENCES

1. Whitcomb, Richard T.: Investigation of the Characteristics of a High-Aspect-Ratio Wing in the Langley 8-Foot High-Speed Tunnel. NACA MR No. L5F09, 1945.

2. Stack, John, and Lindsey, W. F.: Characteristics of Low-Aspect-Ratio Wings at Supercritical Mach Numbers. NACA ACR No. L5J16, 1945.

3. Jones, Robert T.: Wing Plan Forms for High-Speed Flight. NACA TN No. 1033, 1946.

4. Mathews, Charles W., and Thompson, Jim Rogers: Comparative Drag Measurements at Transonic Speeds of Rectangular and Swept-Back NACA 651-009 Airfoils Mounted on a Freely Falling Body. NACA ACR No. L5G30, 1945.

5. Göthert, B.: Hochgeschwindigkeitsmessungen an einem Pfeilflügel (Pfeilwinkel $\varphi = 35°$). Bericht 156 der Lilienthal-Gesellschaft für Luftfahrtforschung, 1942, pp. 30-40.

6. Ludwieg, H.: Versuchsergebnisse. Pfeilflügel bei hohen Geschwindigkeiten. Bericth 127 der Lilienthal-Gesellschaft, 1940, pp. 44-52.

7. Goldstein, S., and Young, A. D.: The Linear Perturbation Theory of Compressible Flow, with Applications to Wind-Tunnel Interference. R. & M. No. 1909, British A.R.C., 1943.

8. Glauert, H.: Wind Tunnel Interference on Wings, Bodies and Airscrews. R. & M. No. 1566, British A.R.C., 1933.

9. Thom, A.: Blockage Corrections and Choking in the R.A.E. High-Speed Tunnel. Rep. No. Aero 1891, British R.A.E., Nov. 1943.

10. Allen, H. Julian, and Vincenti, Walter G.: Wall Interference in a Two-Dimensional-Flow Wind Tunnel with Consideration of the Effect of Compressibility. NACA ARR No. 4K03, 1944.

TABLE I

LIST OF FIGURES AND CONFIGURATIONS

Figure no.	Contents	Configuration	Mach number range
1	Drawing	D-558 model on sting support in the Langley 8-foot high-speed tunnel	
2	Drawing	D-558-1 model	
3	Drawing	Comparison of the Douglas and NACA wing fillet	
4	Drawing	Swept-back model	
5	Drawing	Model with swept-forward wing, original tail, and original fin	
6	Drawing	Model with low-aspect-ratio wing, low-aspect-ratio tail, and original fin	
7	Drawing	Tare setups and evaluation technique	
8	Reynolds number versus M		0.4 to 0.94
9(a)	C_L versus M	Original wing	0.4 to 0.94
9(b)	-----do------	Original wing, original tail, and original fin (D-558-1)	0.4 to 0.94
9(c)	-----do------	Original wing, low-aspect-ratio tail, and original fin	0.4 to 0.94
9(d)	-----do------	Original wing, swept-back tail, and swept-back fin	0.4 to 0.94
10(a)	-----do------	Swept-back wing, low-aspect-ratio tail, and original fin	0.4 to 0.94

TABLE I.- Continued

LIST OF FIGURES AND CONFIGURATIONS - Continued

Figure no.	Contents	Configuration	Mach number range
10(b)	C_L versus M	Swept-back wing, swept-back tail, and swept-back fin	0.4 to 0.94
11(a)	-----do------	Swept-forward wing	0.4 to 0.94
11(b)	-----do------	Swept-forward wing, original tail, and original fin	0.4 to 0.94
11(c)	-----do------	Swept-forward wing, low-aspect-ratio tail, and original fin	0.4 to 0.94
12(a)	-----do------	Low-aspect-ratio wing	0.4 to 0.94
12(b)	-----do------	Low-aspect-ratio wing, original tail, and original fin	0.4 to 0.94
12(c)	-----do------	Low-aspect-ratio wing, low-aspect-ratio tail, and original fin	0.4 to 0.94
12(d)	-----do------	Low-aspect-ratio wing, swept-back tail, and swept-back fin	0.4 to 0.94
13	-----do------	Complete original (D-558-1), Complete swept-back Low-aspect-ratio wing, low-aspect ratio tail, and original fin Swept-forward wing, originl tail and original fin Wing NACA 65-210; A = 9 (reference 1)	0.4 to 0.94
14(a)	dC_L/d_α versus M	Complete original	0.4 to 0.925

TABLE I.- Continued

LIST OF FIGURES AND CONFIGURATIONS - Continued

Figure no.	Contents	Configuration	Mach number range
14(b)	$dC_L/d\alpha$ versus M	Low-aspect-ratio wing, low-aspect-ratio tail, and original fin	0.4 to 0.925
14(c)	------do-------	Complete swept back	0.4 to 0.925
14(d)	------do-------	Swept-forward wing, original tail, and original fin	0.4 to 0.925
15	C_L versus M	Level flight lift coefficients required at sea level and 35,000 ft altitude for a wing loading of 53.9 pounds per square foot	0.3 to 1.0
16	$\alpha C_L = 0$ versus M	Complete original (D-558-1) Complete swept back Low-aspect-ratio wing, low-aspect-ratio tail, and original fin Swept-forward wing, original tail and original fin Wing NACA 65-210; A = 9 (reference 1)	0.4 to 0.94
17(a)	C_D versus M	Original wing and original fin	0.4 to 0.9
17(b)	--------do-------	Original wing, original tail, and original fin (D-558-1)	0.4 to 0.9
17(c)	--------do-------	Original wing, low-aspect-ratio tail, and original fin	0.4 to 0.9
17(d)	--------do-------	Swept-back wing, swept-back tail, and swept-back fin	0.4 to 0.91

TABLE I. - Concluded

LIST OF FIGURES AND CONFIGURATIONS - Concluded

Figure no.	Contents	Configuration	Mach number range
18(a)	C_L versus C_D	Complete original (D-558-1) and complete swept back	0.4
18(b)	-------do---------	----------do----------	0.6
18(c)	-------do---------	----------do----------	0.7
18(d)	-------do---------	----------do----------	0.8
18(e)	-------do---------	----------do----------	0.85
18(f)	-------do---------	----------do----------	0.9
19(a)	C_D versus M, C_L = 0.4	Complete original (D-558-1), complete swept back, and wing NACA 65-210, A = 9 (reference 1)	0.4 to 0.91
19(b)	C_D versus M, C_L = 0.1	----------do----------	0.4 to 0.91
20	L/D versus C_L	Complete original (D-558-1) and complete swept back	0.4 to 0.9
21	L/D_{max} versus M	Complete original (D-558-1) and complete swept back	0.4 to 0.9

NATIONAL ADVISORY
COMMITTEE FOR AERONAUTICS

TABLE II

WING AND TAIL DIMENSIONS OF $\frac{1}{16}$-SCALE MODEL

	Original D-558-1	Swept back	Low aspect ratio	Swept forward
Wing section	65_1-110	65_1-110	65_1-110	65_1-110
Wing aspect ratio	4.17	4.17	2.00	4.17
Wing taper ratio	1.85	1.85	1.85	1.85
Wing span, in.	18.76	18.76	13.00	18.76
Wing area, sq ft	0.587	0.587	0.587	0.587
Wing mean aerodynamic chord, in.	4.656	4.656	6.687	4.656
Wing incidence angle	2.0°	2.0°	2.5°	2.0°
Wing dihedral	4.0°	4.0°	4.0°	4.0°
Wing sweep angle (50-percent chord)	0°	35°	0°	-35°
Wing root chord	5.88	5.94	8.44	5.94
Wing tip chord	3.17	3.20	4.55	3.20
Longitudinal location of 25-percent mean aerodynamic chord point from nose - inlet station, in.	11.96	11.96	11.96	11.96
Tail section	65_1-008	65_1-008	65_1-008	
Tail aspect ratio	4.17	4.17	2.0	
Tail taper ratio	1.821	1.80	1.80	
Tail span, in.	9.19	9.18	6.50	
Tail area, sq ft	0.140	0.140	0.142	
Tail dihedral	0°	0°	0°	
Tail sweep angle (50-percent chord)	0°	35°	0°	
Elevator area, percent of tail area	25	25	25	

NATIONAL ADVISORY
COMMITTEE FOR AERONAUTICS

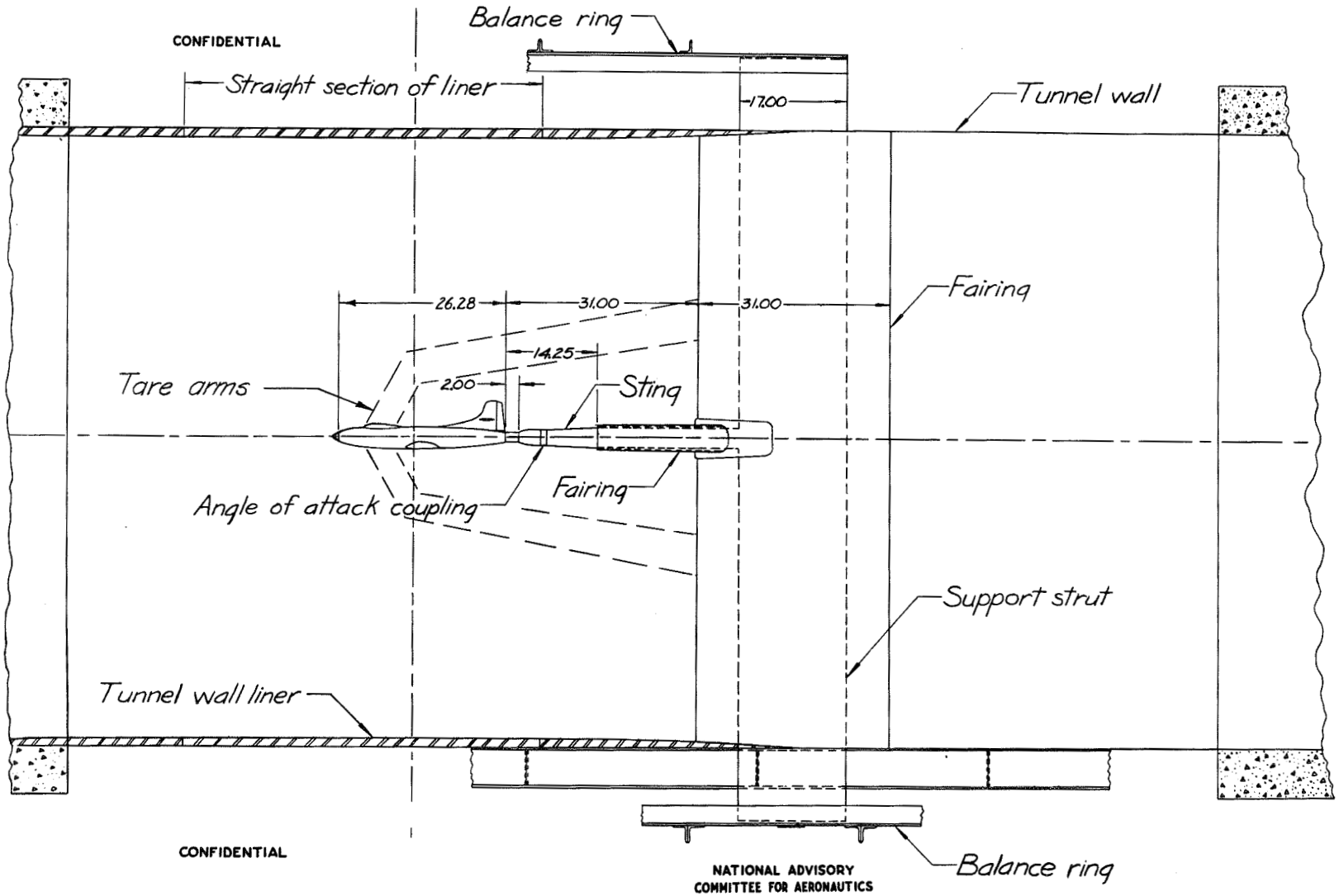

Figure 1.- D-558 model on sting support in the Langley 8-foot high-speed tunnel.

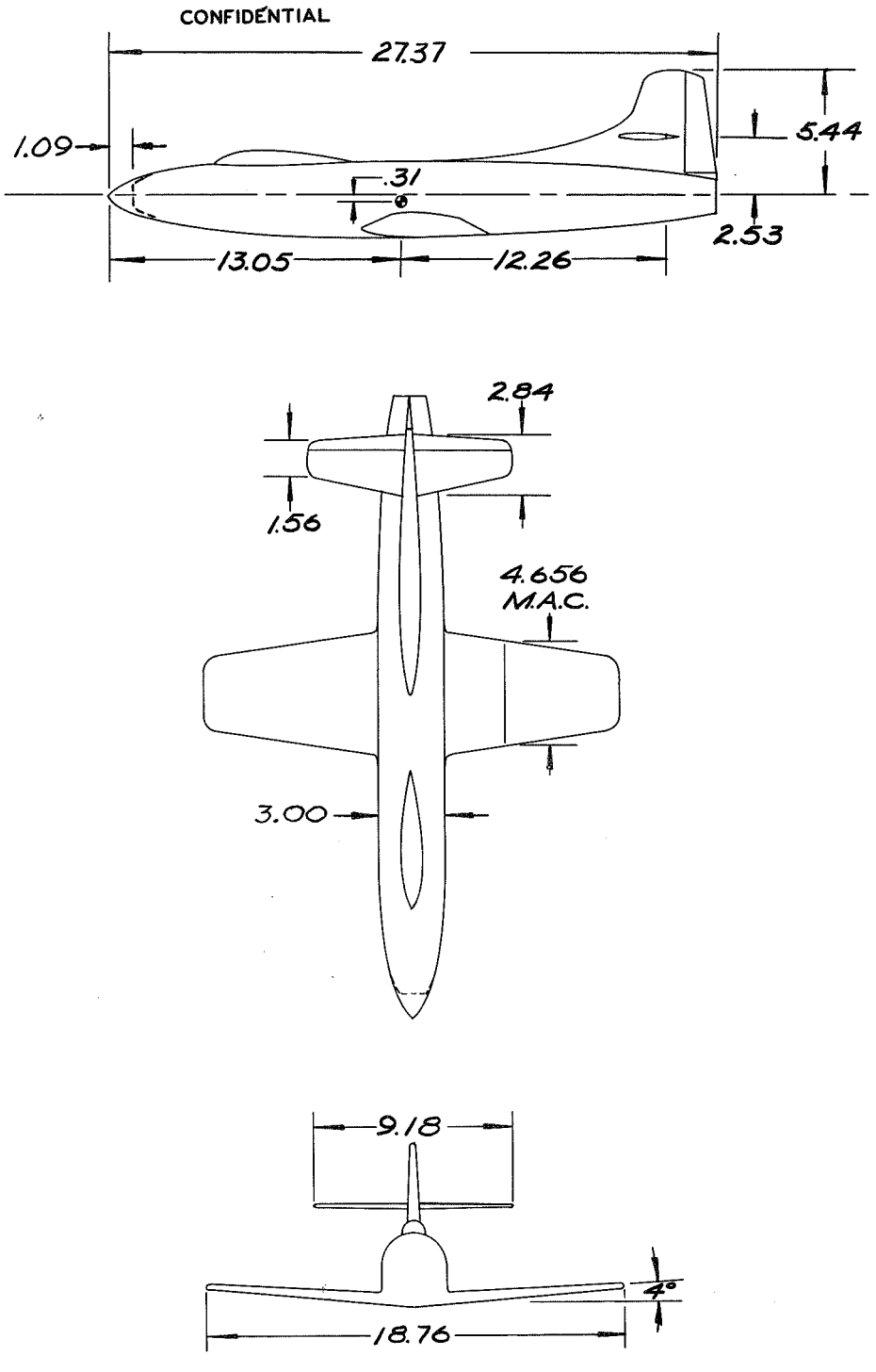

Figure 2.- Drawing of 1/16 scale D-558-1 model as tested in the Langley 8-foot high-speed tunnel. All dimensions in inches.

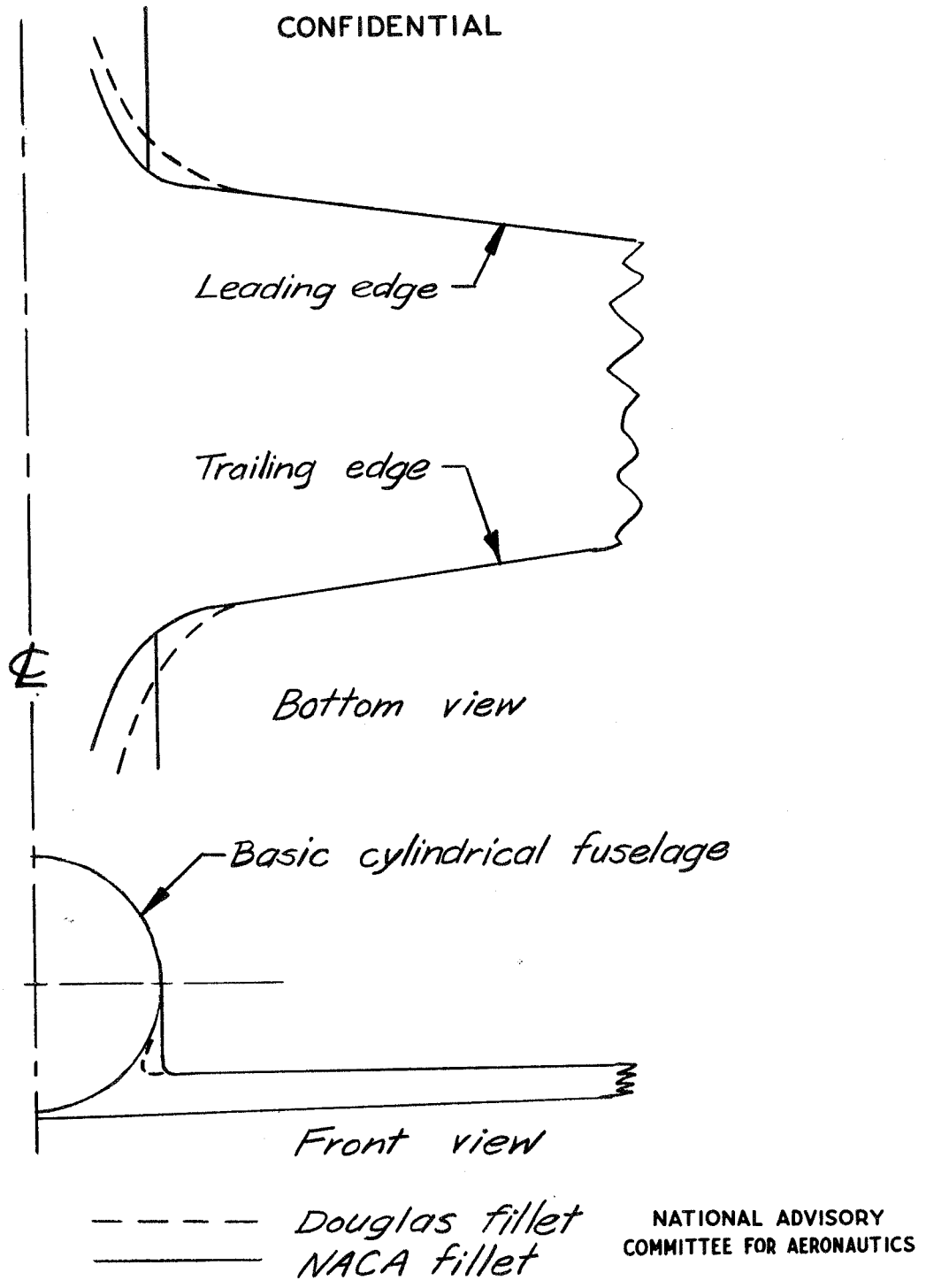

Figure 3 .-Approximate comparison of the Douglas and NACA wing fillet.

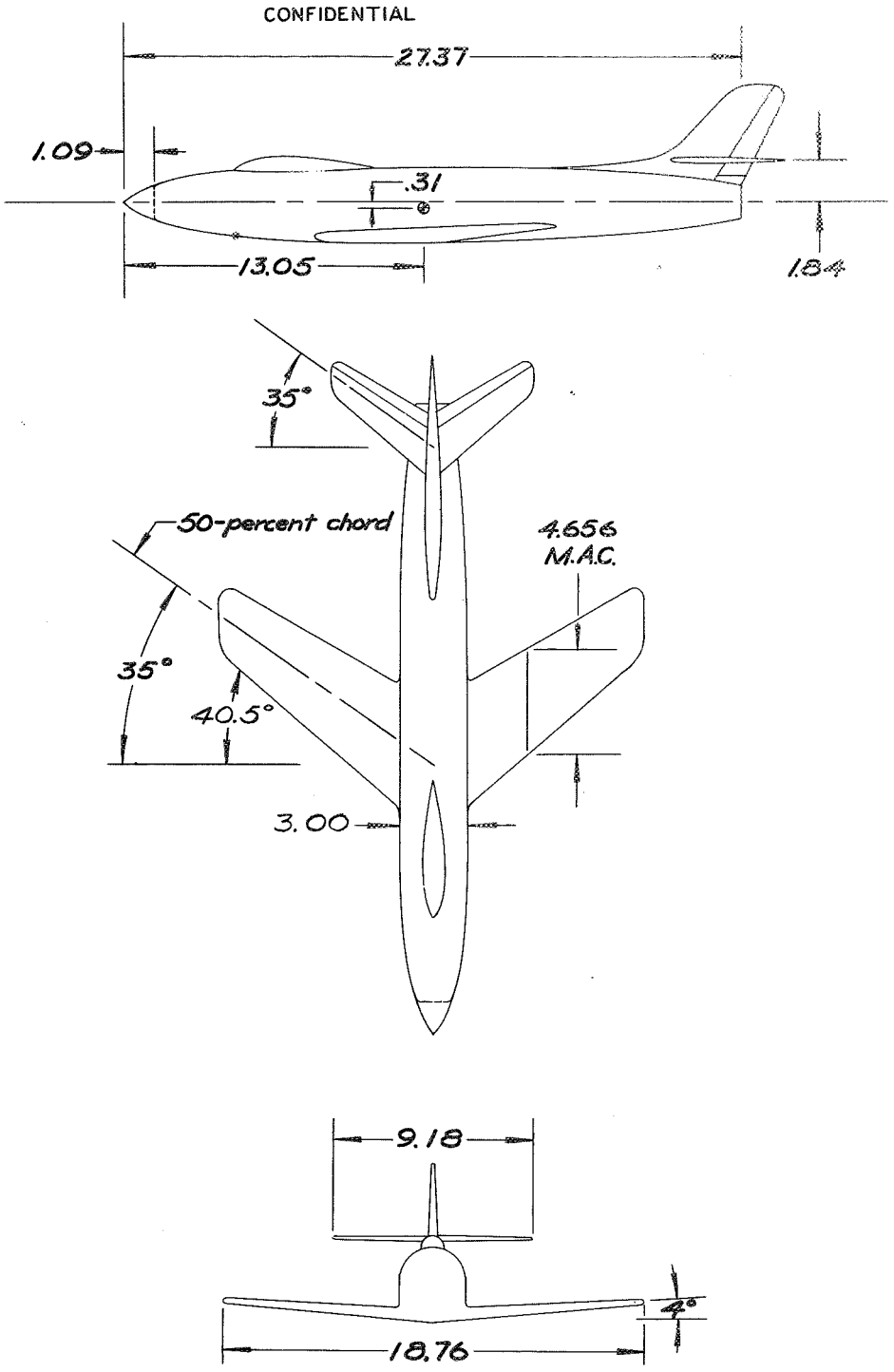

Figure 4.— Drawing of 1/16 scale sweptback model as tested in the Langley 8-foot high-speed tunnel. All dimensions in inches.

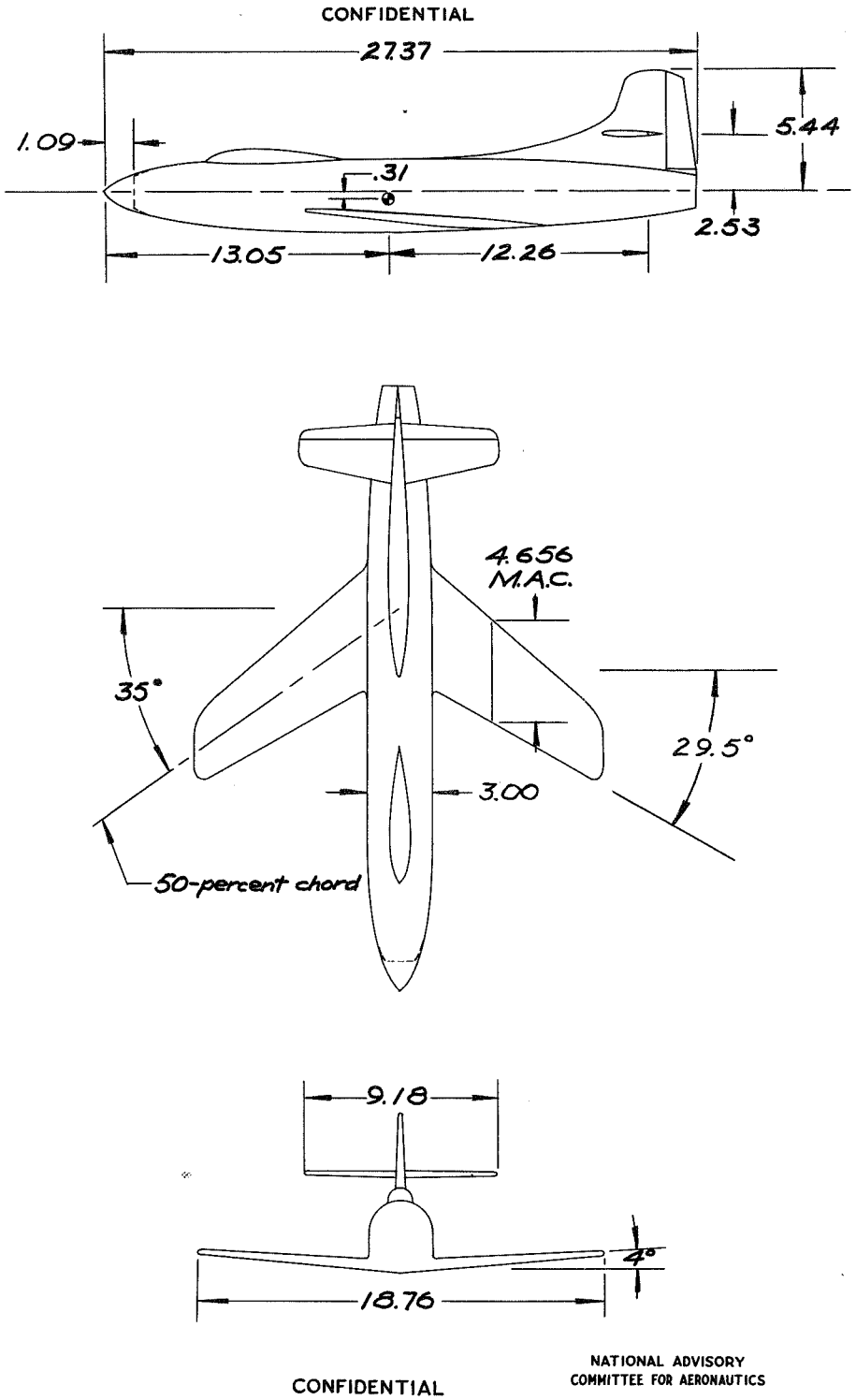

Figure 5 .- Drawing of 1/16 scale D-558 model with sweptforward wing, original tail, and original fin as tested in the Langley 8-foot high-speed tunnel. All dimensions in inches.

CONFIDENTIAL

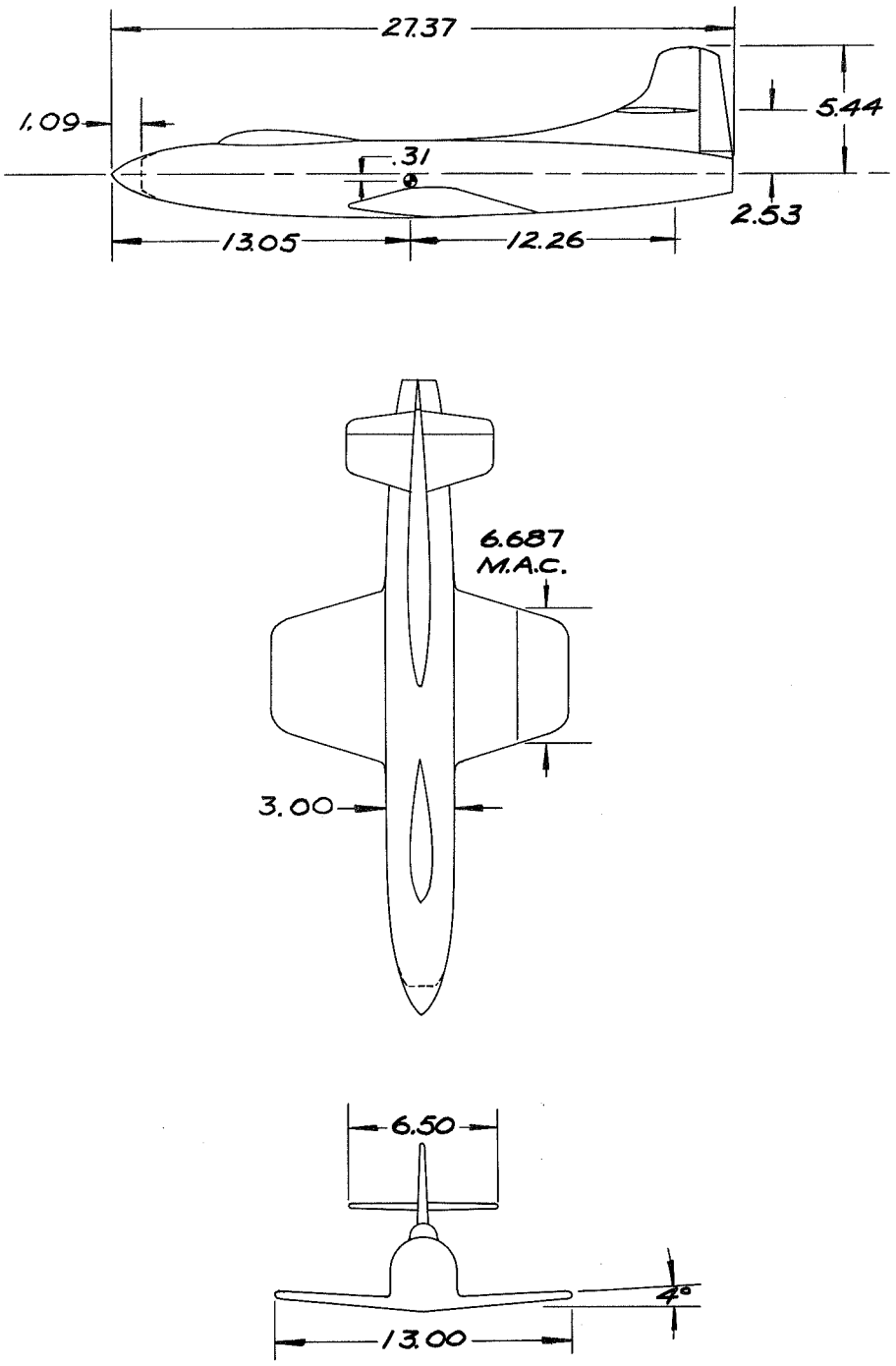

NATIONAL ADVISORY
COMMITTEE FOR AERONAUTICS

CONFIDENTIAL

Figure 6.- Drawing of 1/16 scale D-558 model with low-aspect-ratio wing, low-aspect-ratio tail, and original fin as tested in the Langley 8-foot high-speed tunnel. All dimensions in inches.

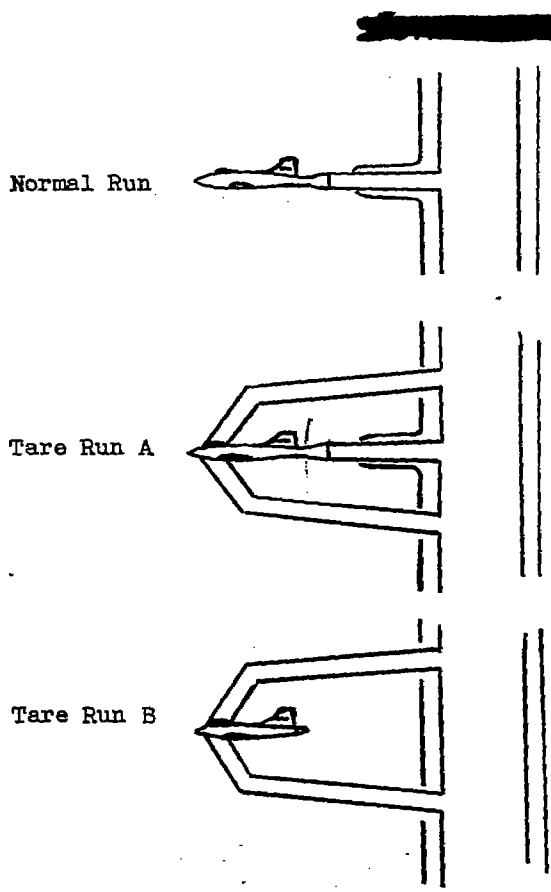

	Balance Ring Measures
Normal Run	Model force Sting force Interference of sting on model Interference of model on sting
Tare Run A	Model force Sting force Tare-arm force Guy-wire force Mutual interference of model and arms Interference of sting on model Interference of model on sting
Tare Run B	Model force Tare-arm force Guy-wire force Mutual interference of model and arms
Tare Run A—Tare Run B	Sting force Interference of sting on model Interference of model on sting
Normal Run—(A — B)	Model force

NATIONAL ADVISORY
COMMITTEE FOR AERONAUTICS

Figure 7.- Tare setups and evaluation technique.

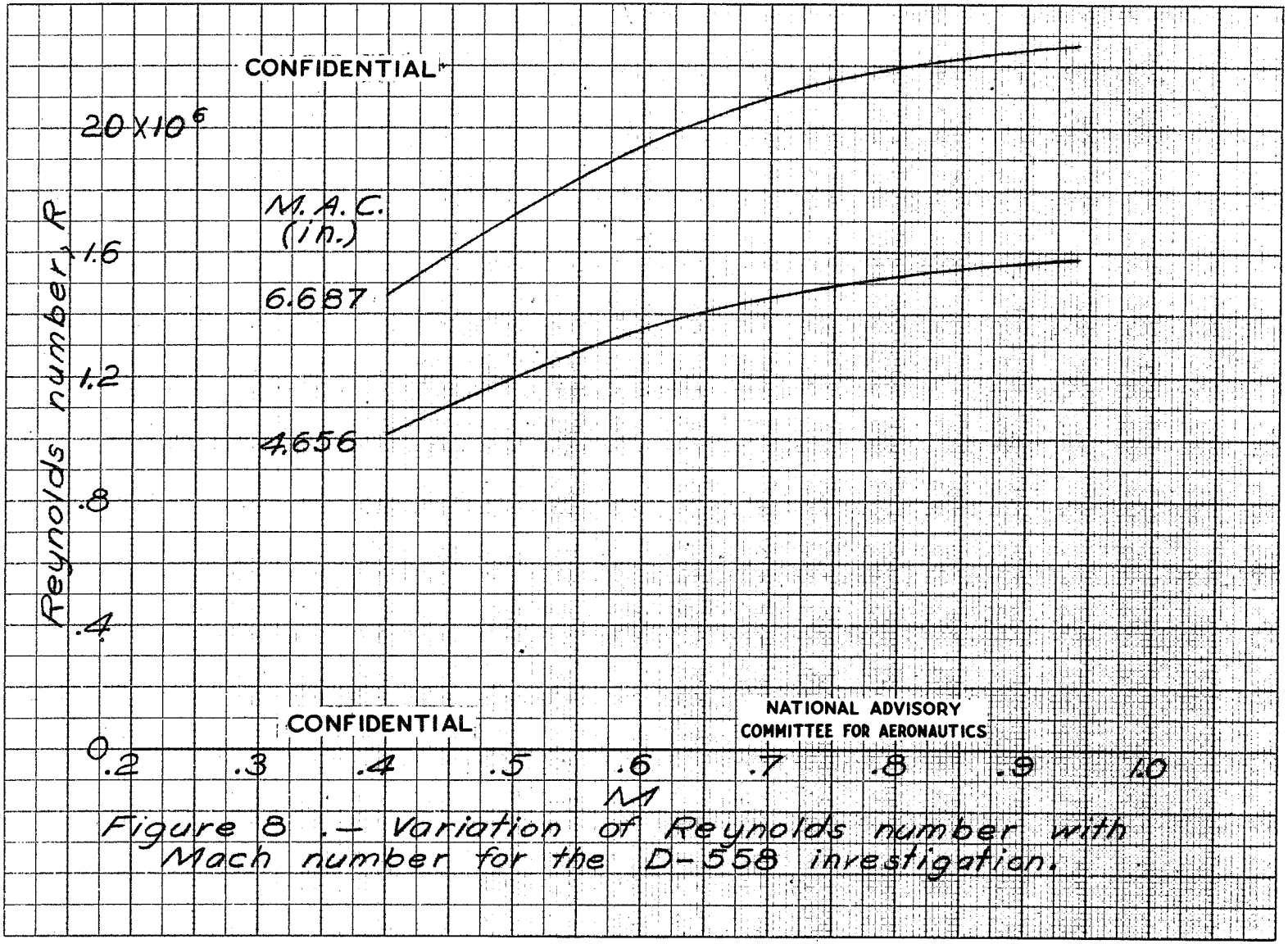

Figure 8 .— Variation of Reynolds number with Mach number for the D-558 investigation.

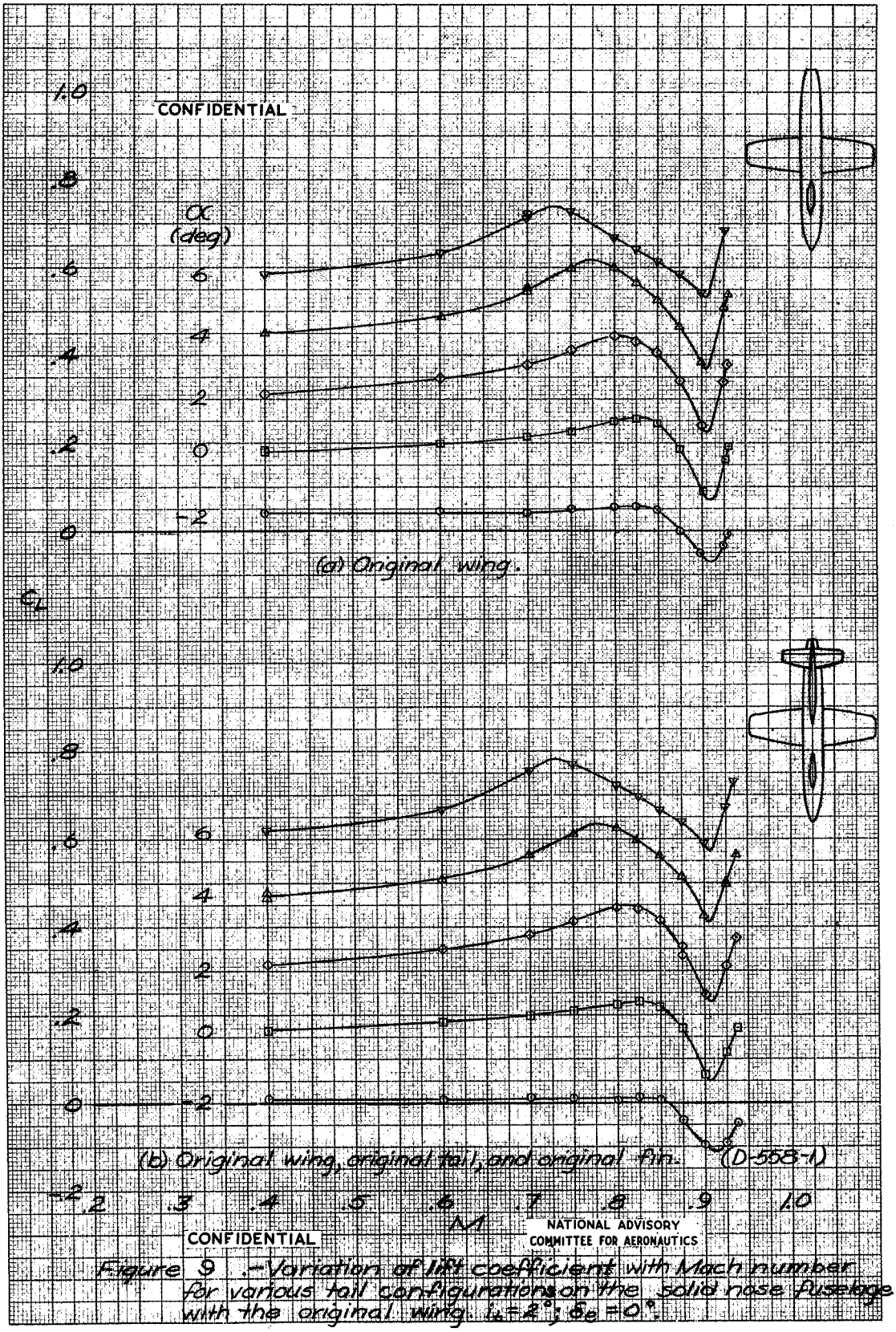

Figure 9.--Variation of lift coefficient with Mach number for various tail configurations on the solid nose fuselage with the original wing. $i_t = 2°$; $\delta_e = 0°$.

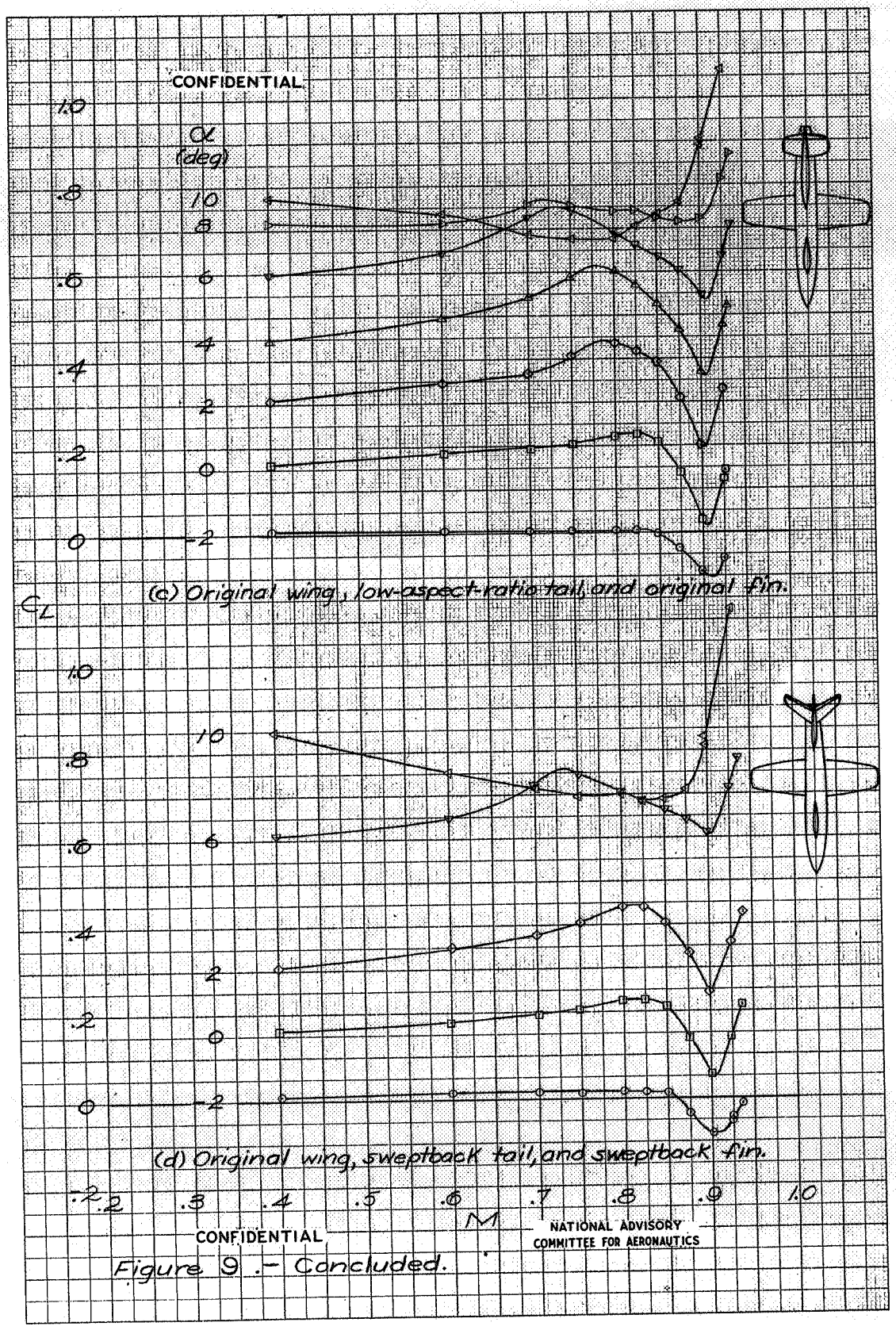

Figure 9.- Concluded.

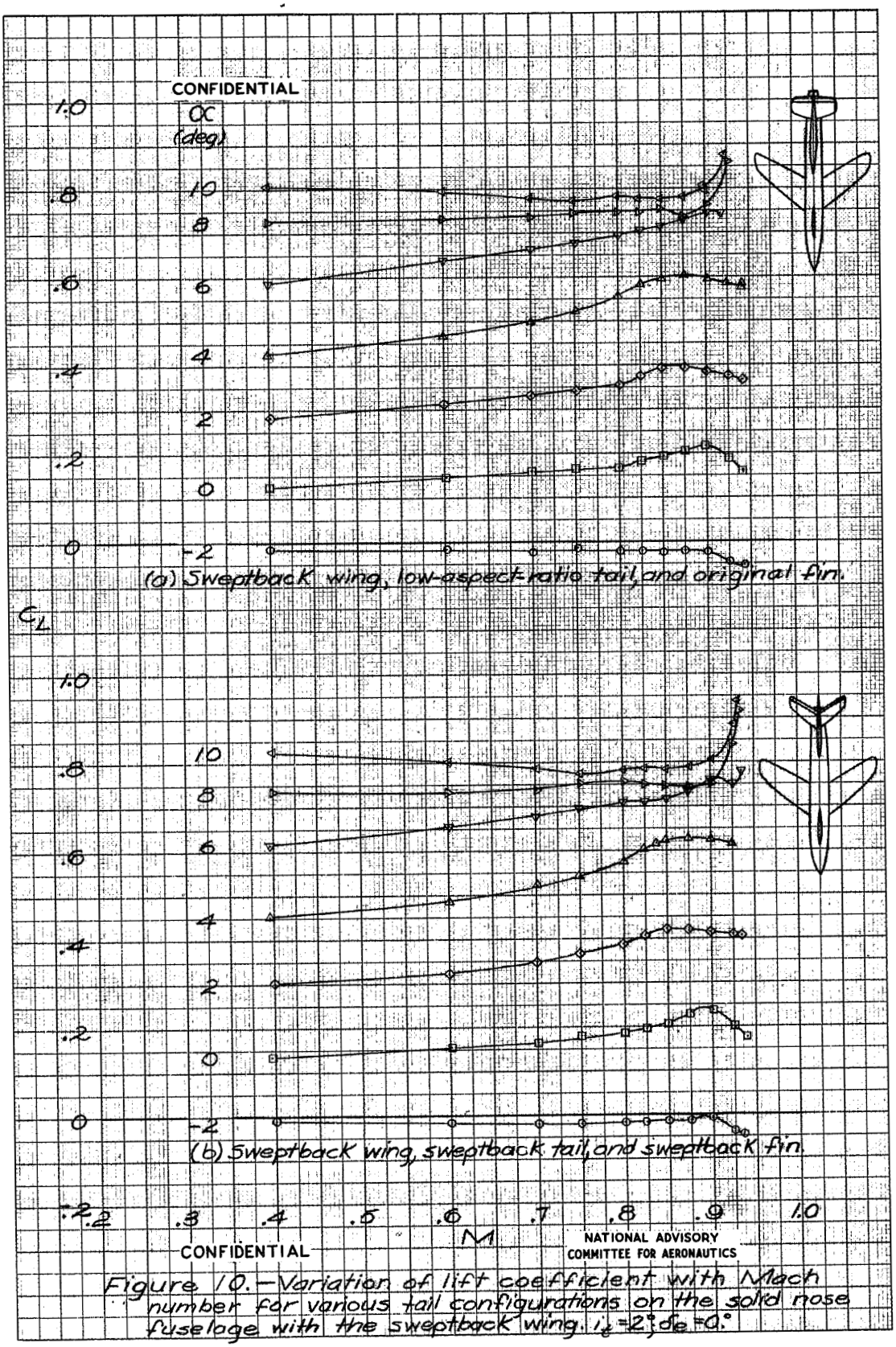

Figure 10.—Variation of lift coefficient with Mach number for various tail configurations on the solid nose fuselage with the sweptback wing. $i_t = 2°$; $\delta_e = 0°$.

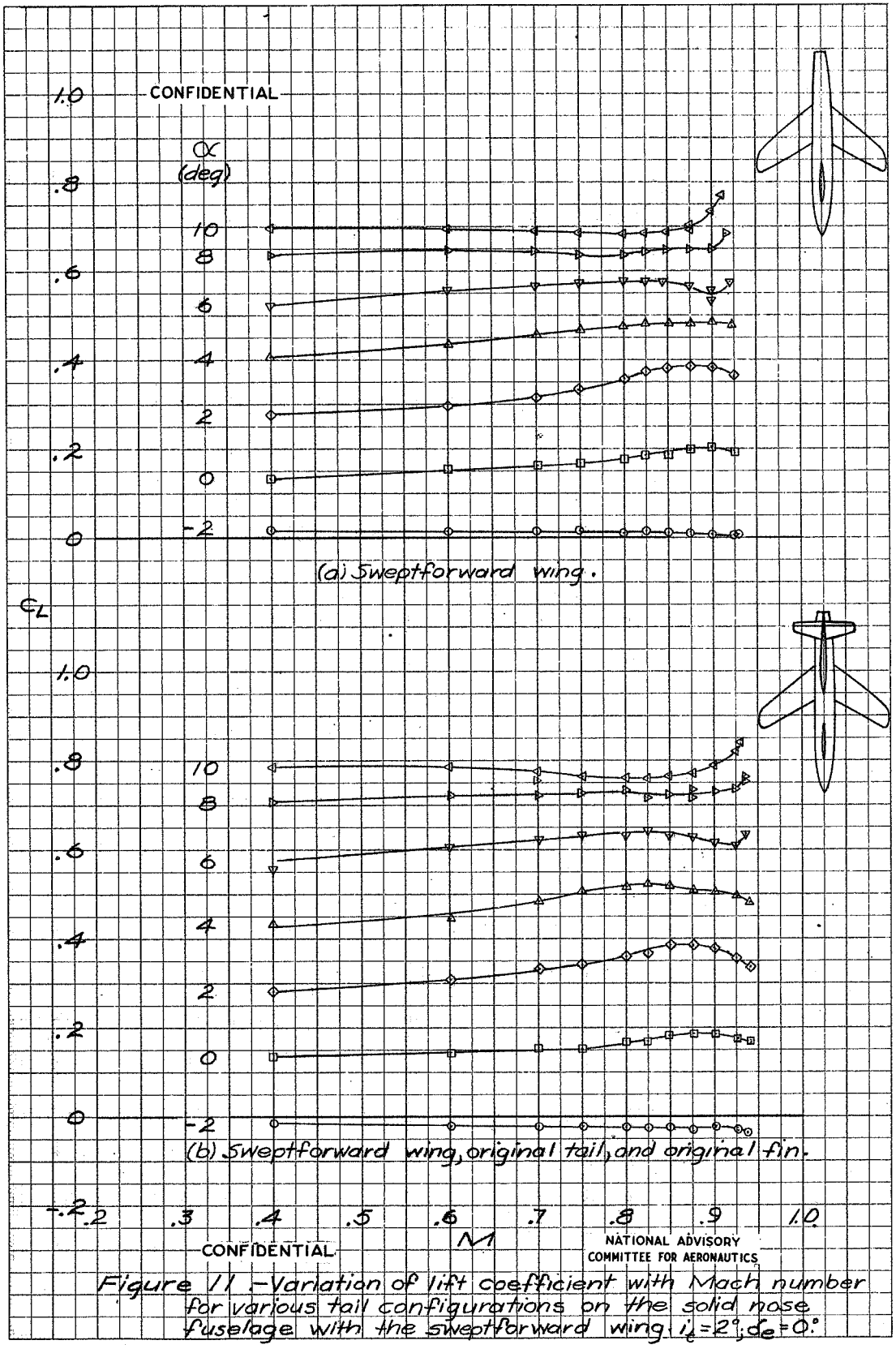

Figure 11.-Variation of lift coefficient with Mach number for various tail configurations on the solid nose fuselage with the sweptforward wing. $i_t = 2°$; $\delta_e = 0°$.

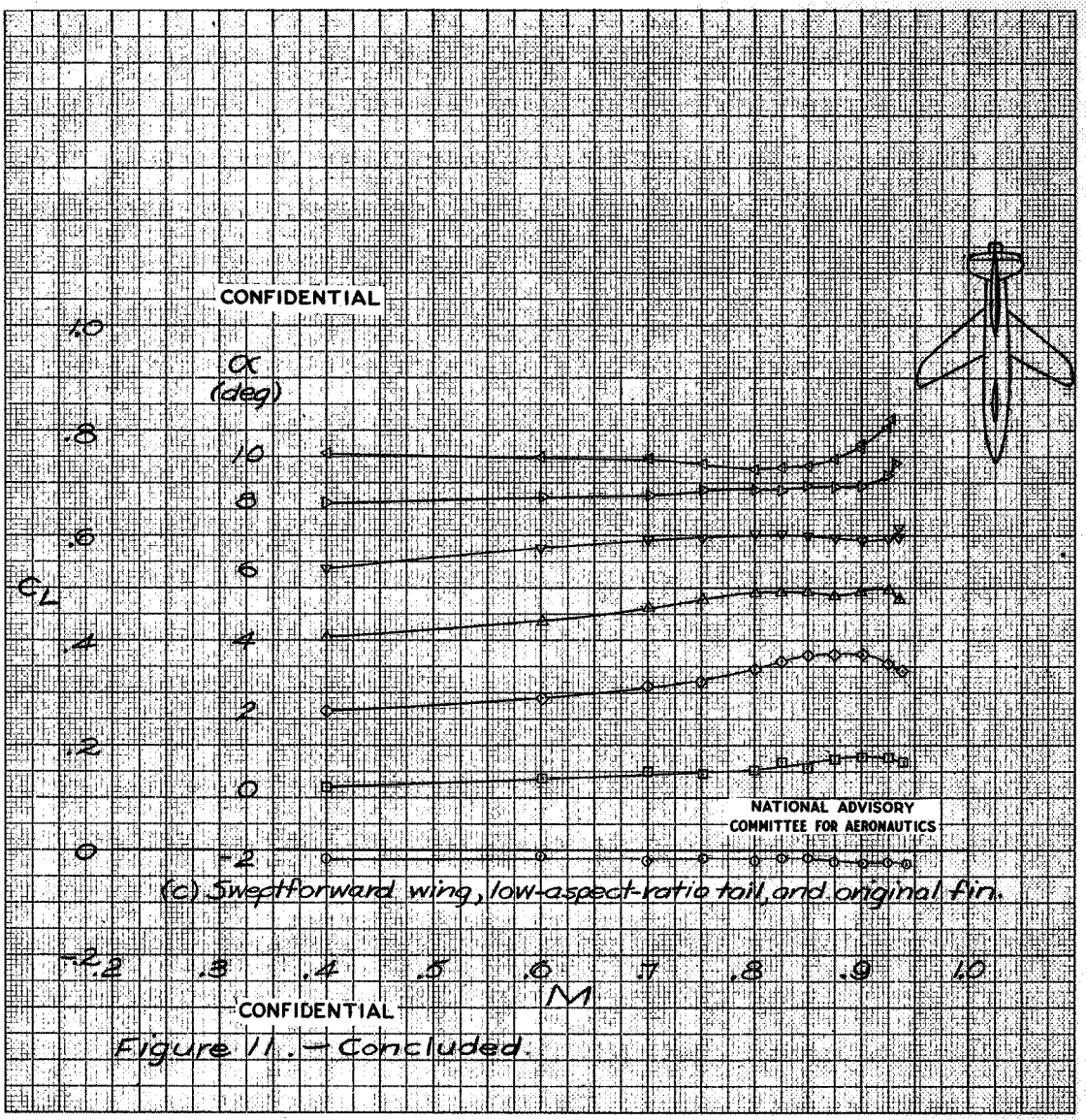

(c) Sweptforward wing, low-aspect-ratio tail, and original fin.

Figure 11.- Concluded.

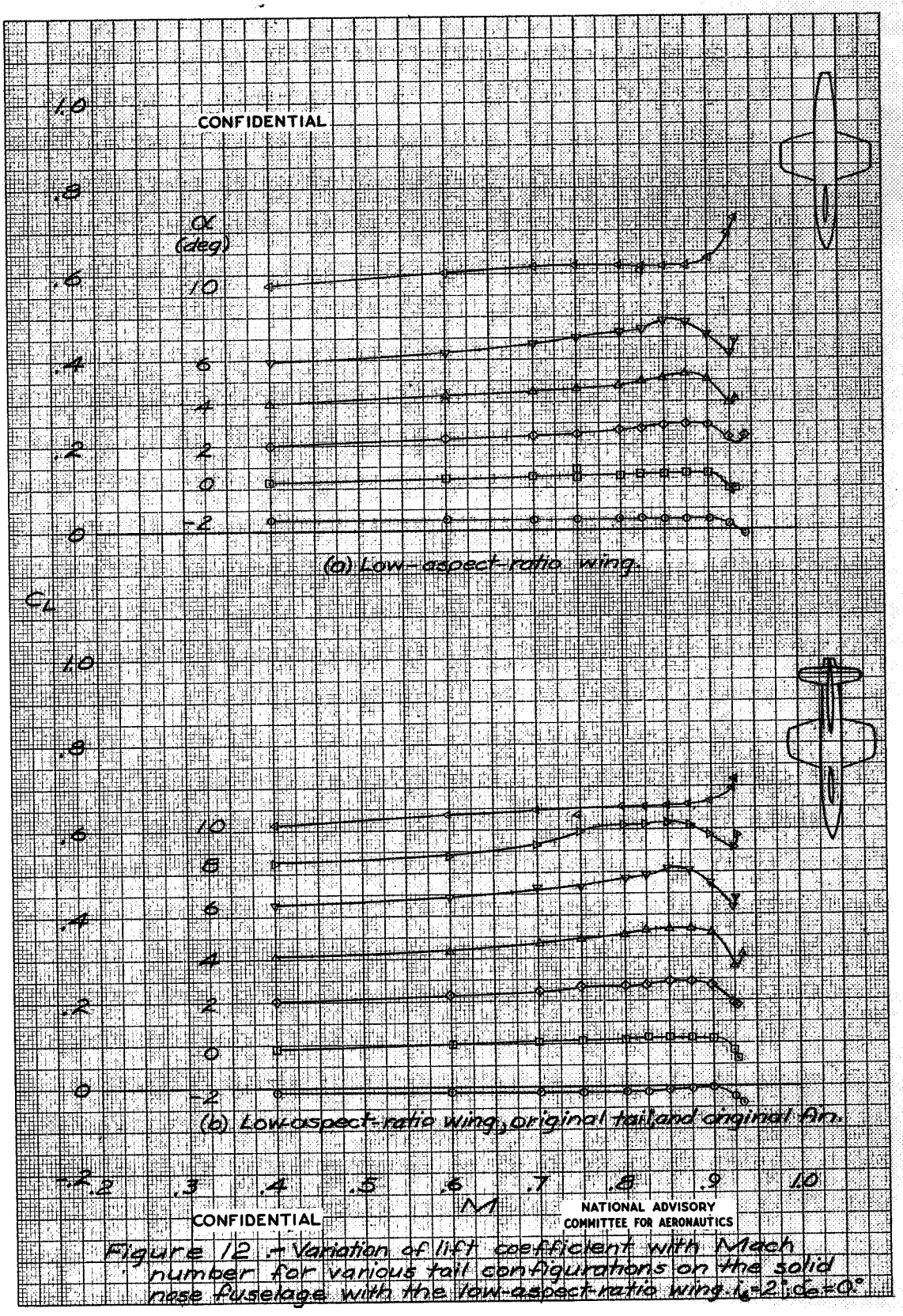

Figure 12.- Variation of lift coefficient with Mach number for various tail configurations on the solid nose fuselage with the low-aspect-ratio wing. i_t=-2°; δ_e=0°.

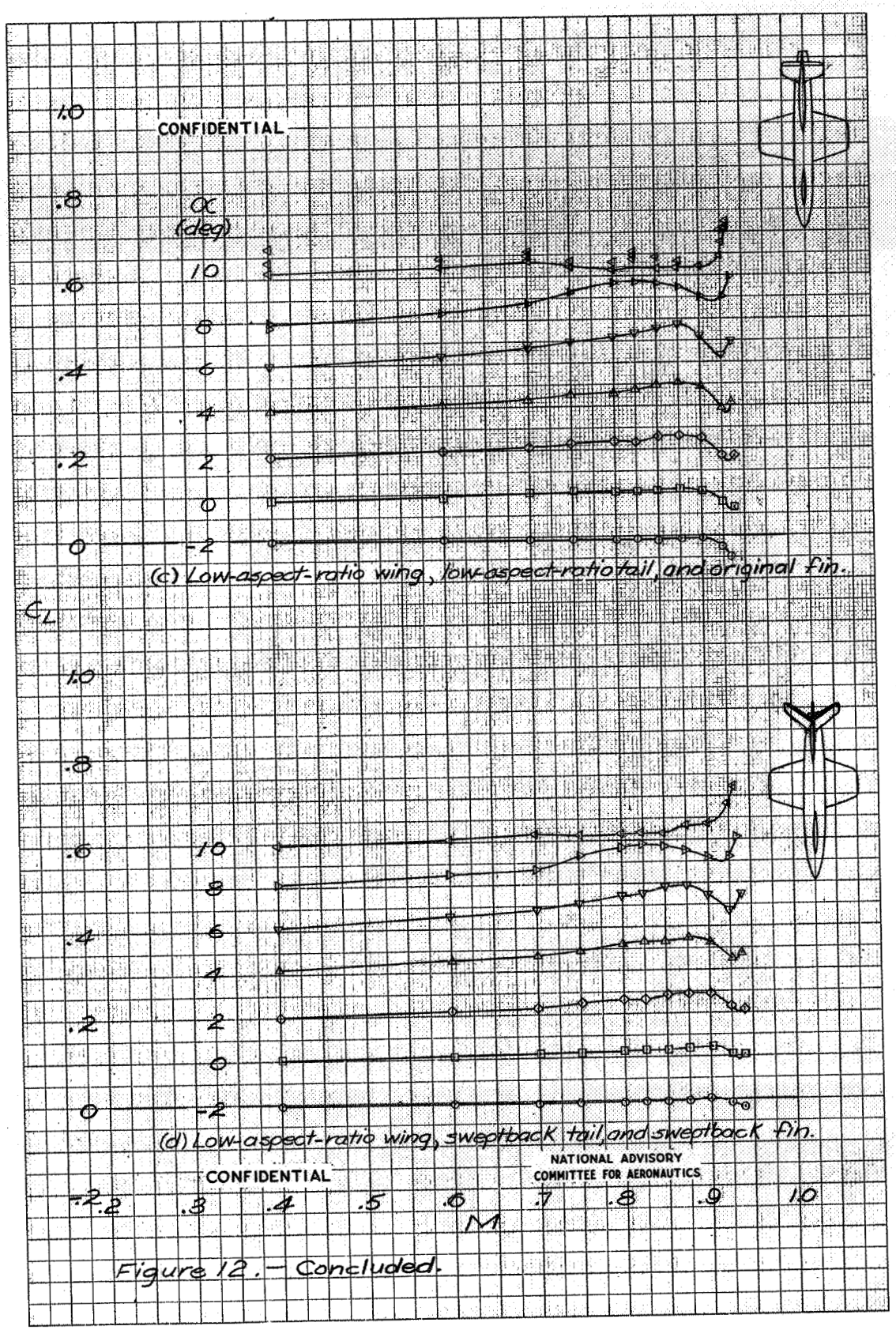

Figure 12.- Concluded.

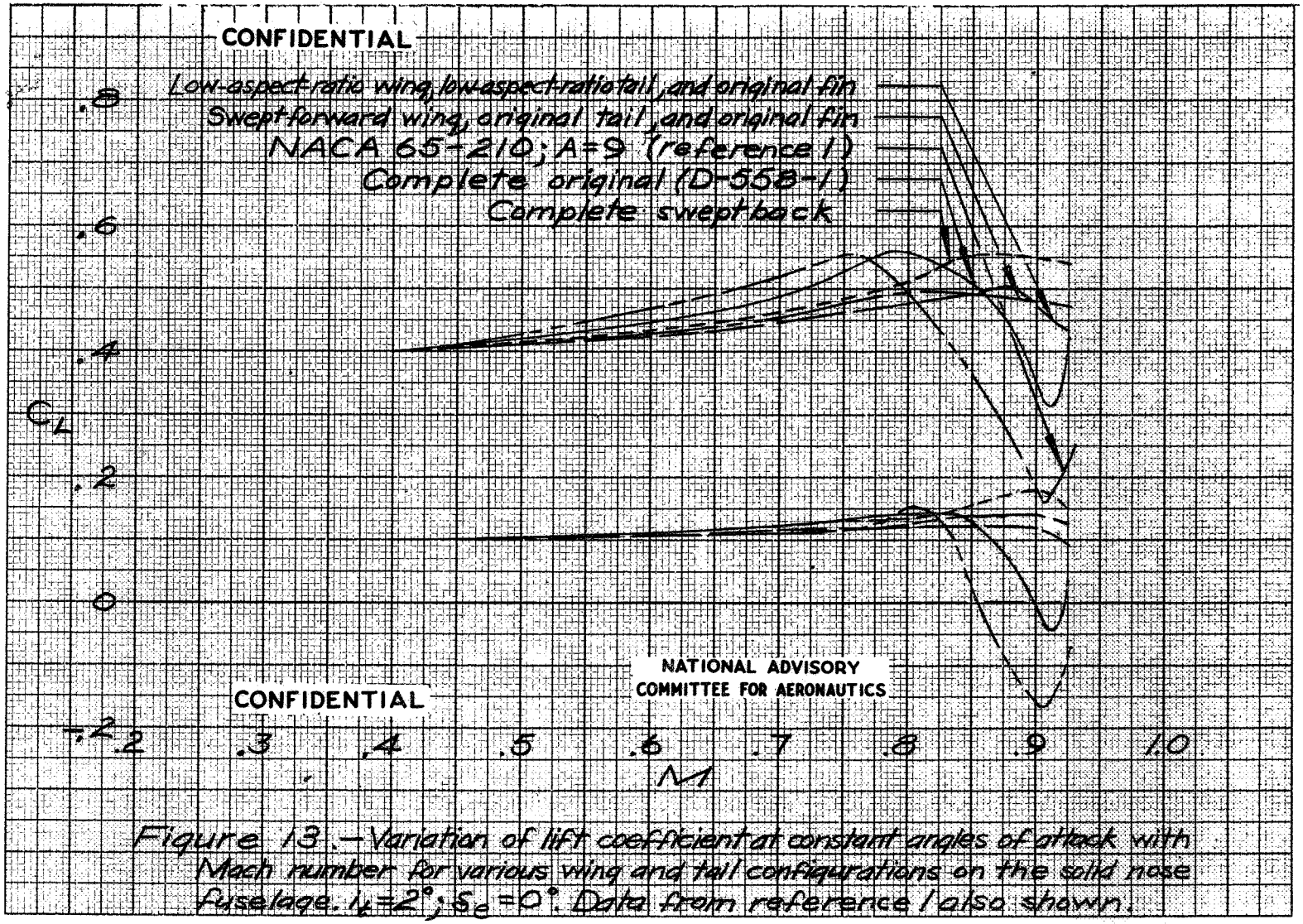

Figure 13.—Variation of lift coefficient at constant angles of attack with Mach number for various wing and tail configurations on the solid nose fuselage. $i_t = 2°$; $\delta_e = 0°$. Data from reference 1 also shown.

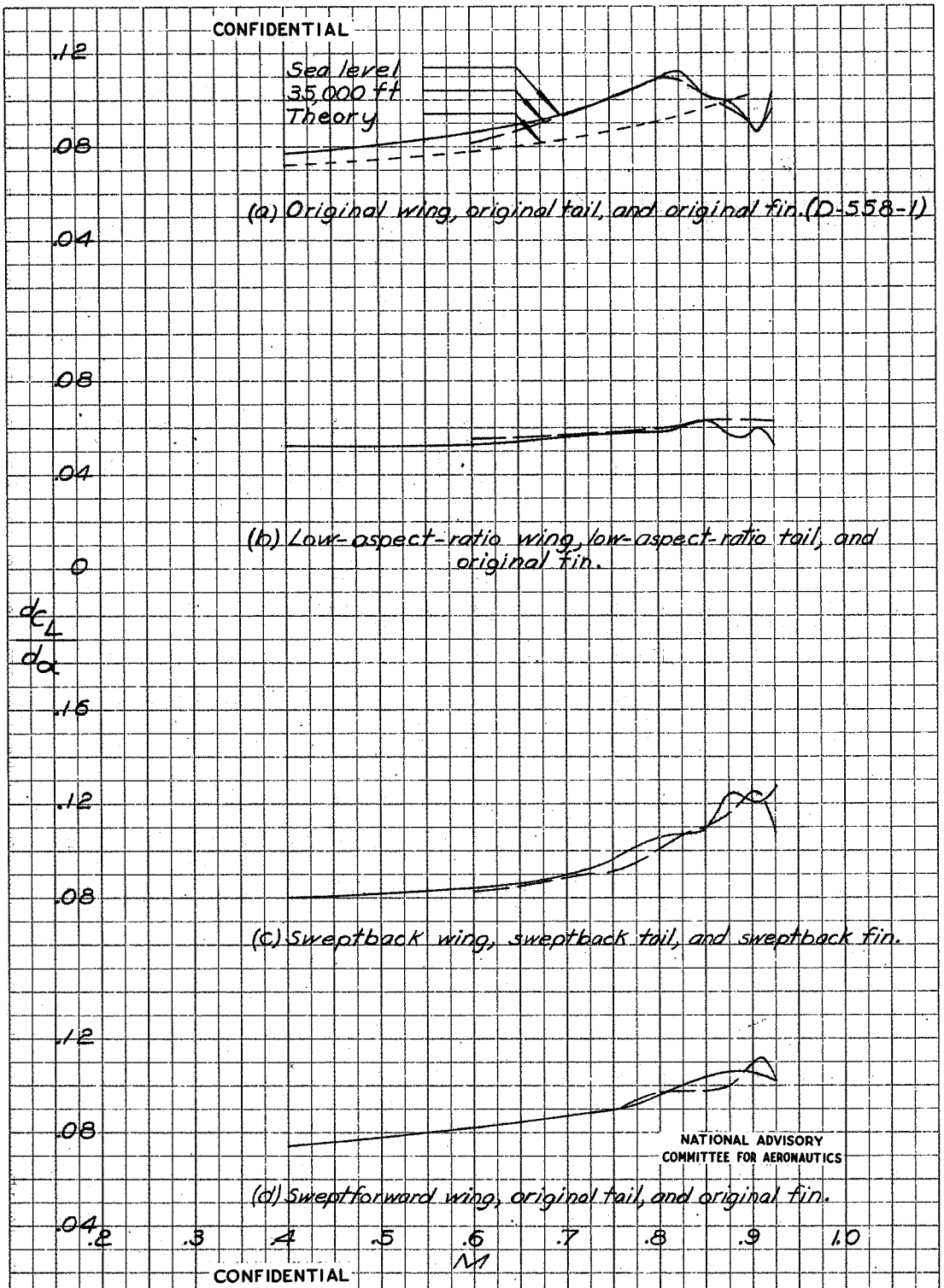

Figure 14.—Variation of slope of lift curves with Mach number for various configurations at level-flight lift coefficients, based on a wing loading of 50 pounds per square foot, at sea level and 35,000 feet altitude. $i_t = 2°$; $\delta_e = 0°$.

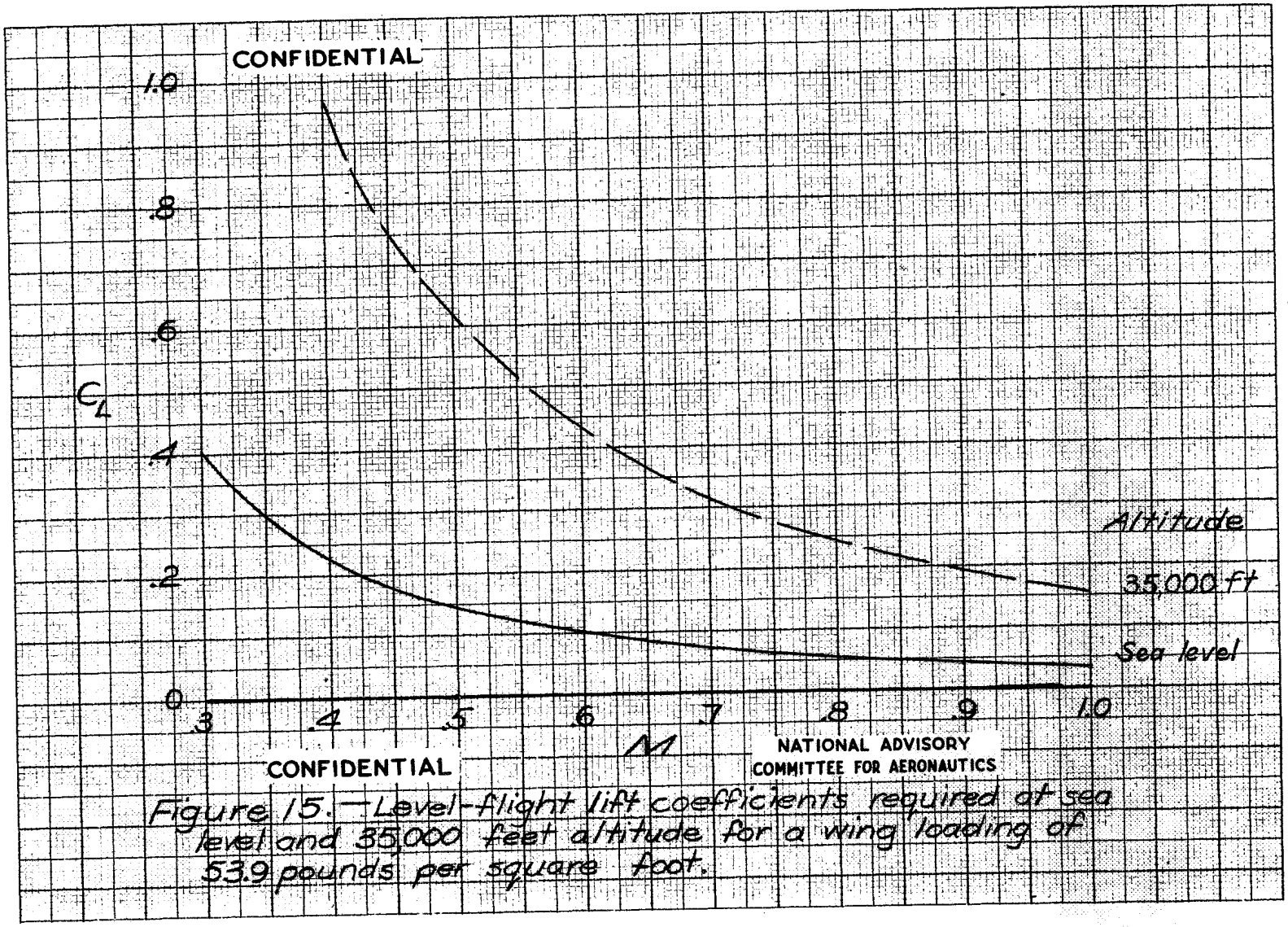

Figure 15.—Level-flight lift coefficients required at sea level and 35,000 feet altitude for a wing loading of 53.9 pounds per square foot.

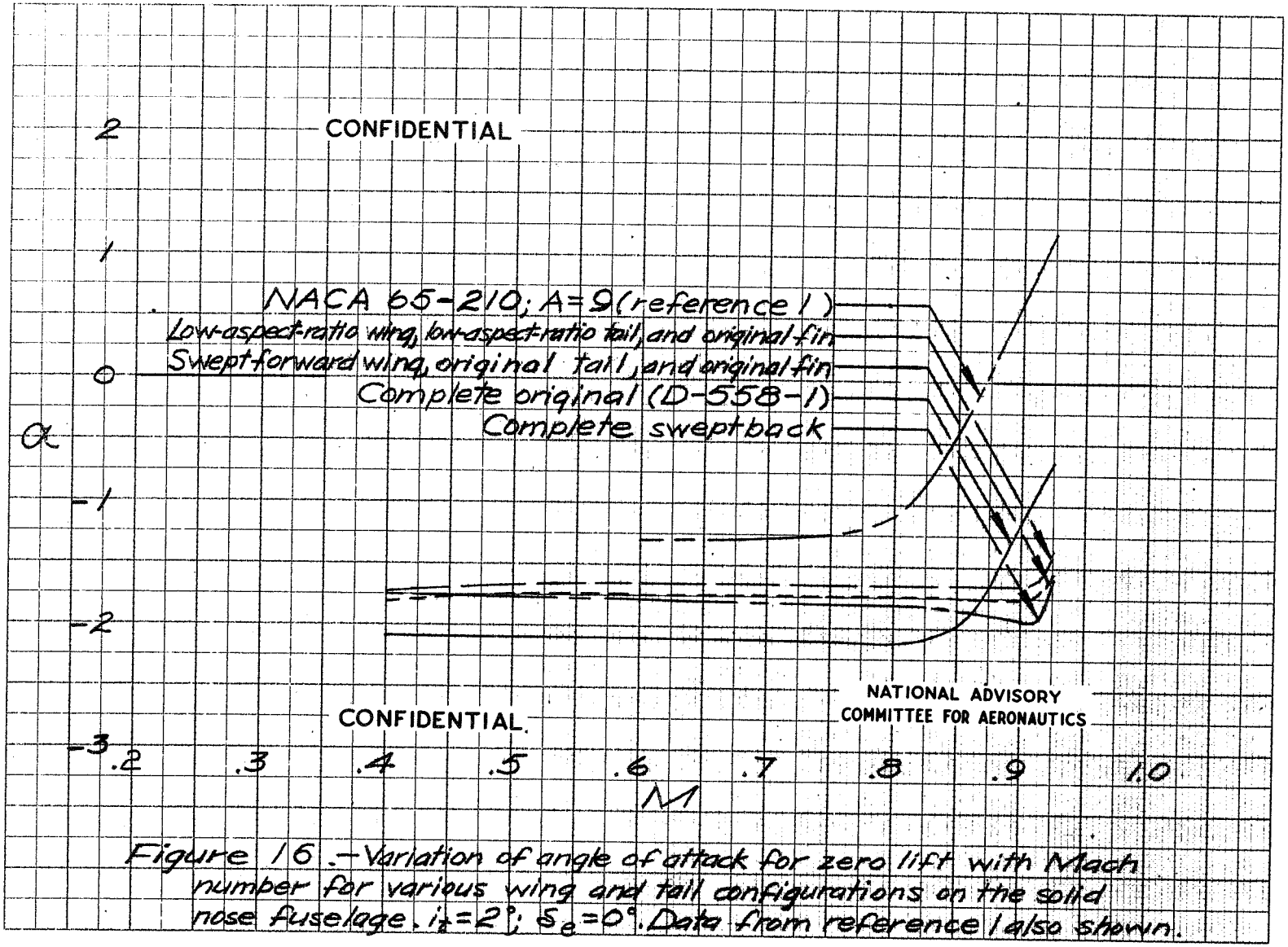

Figure 16.—Variation of angle of attack for zero lift with Mach number for various wing and tail configurations on the solid nose fuselage. $i_t = 2°$; $\delta_e = 0°$. Data from reference 1 also shown.

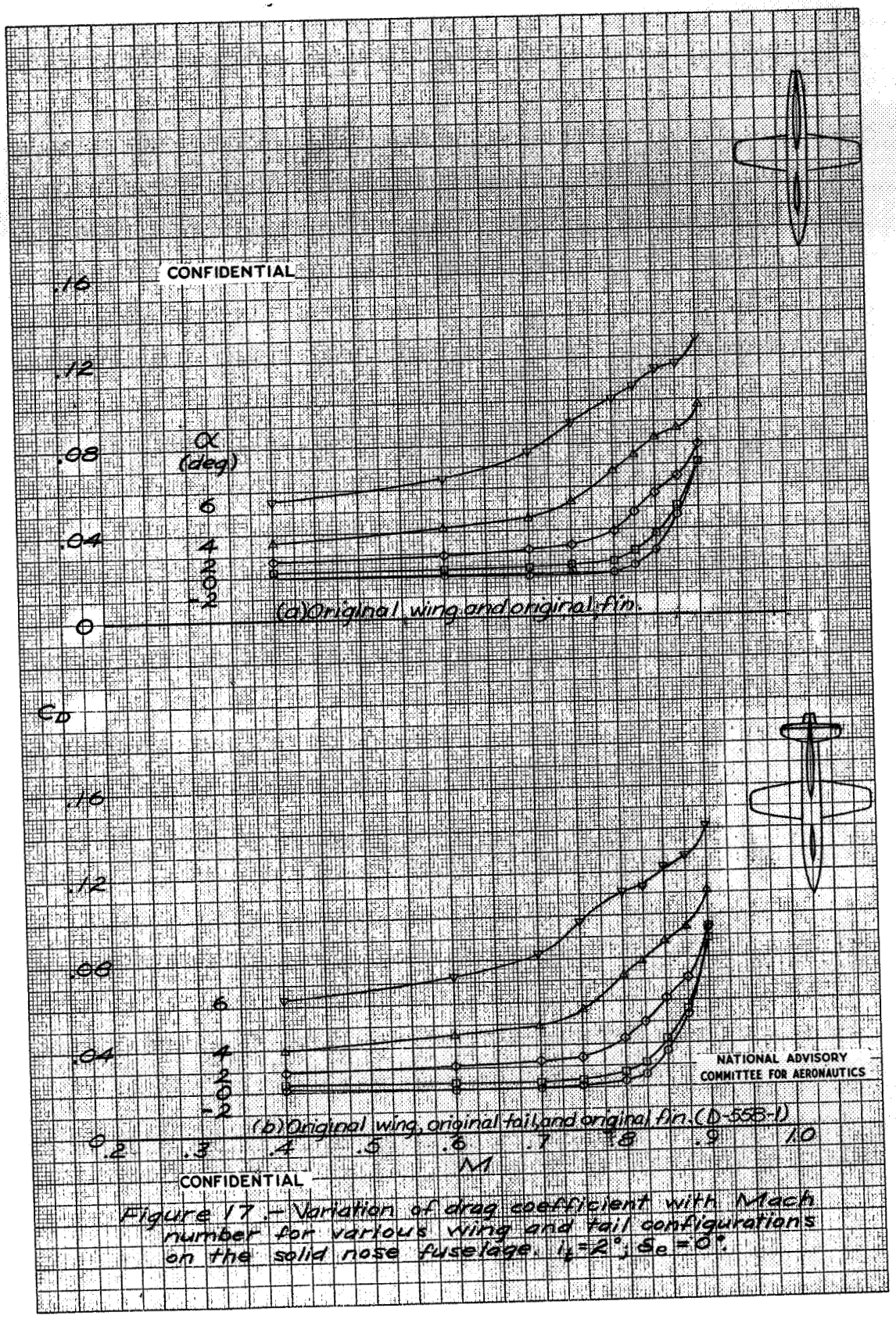

Figure 17.- Variation of drag coefficient with Mach number for various wing and tail configurations on the solid nose fuselage. $i_t = 2°$; $\delta_e = 0°$.

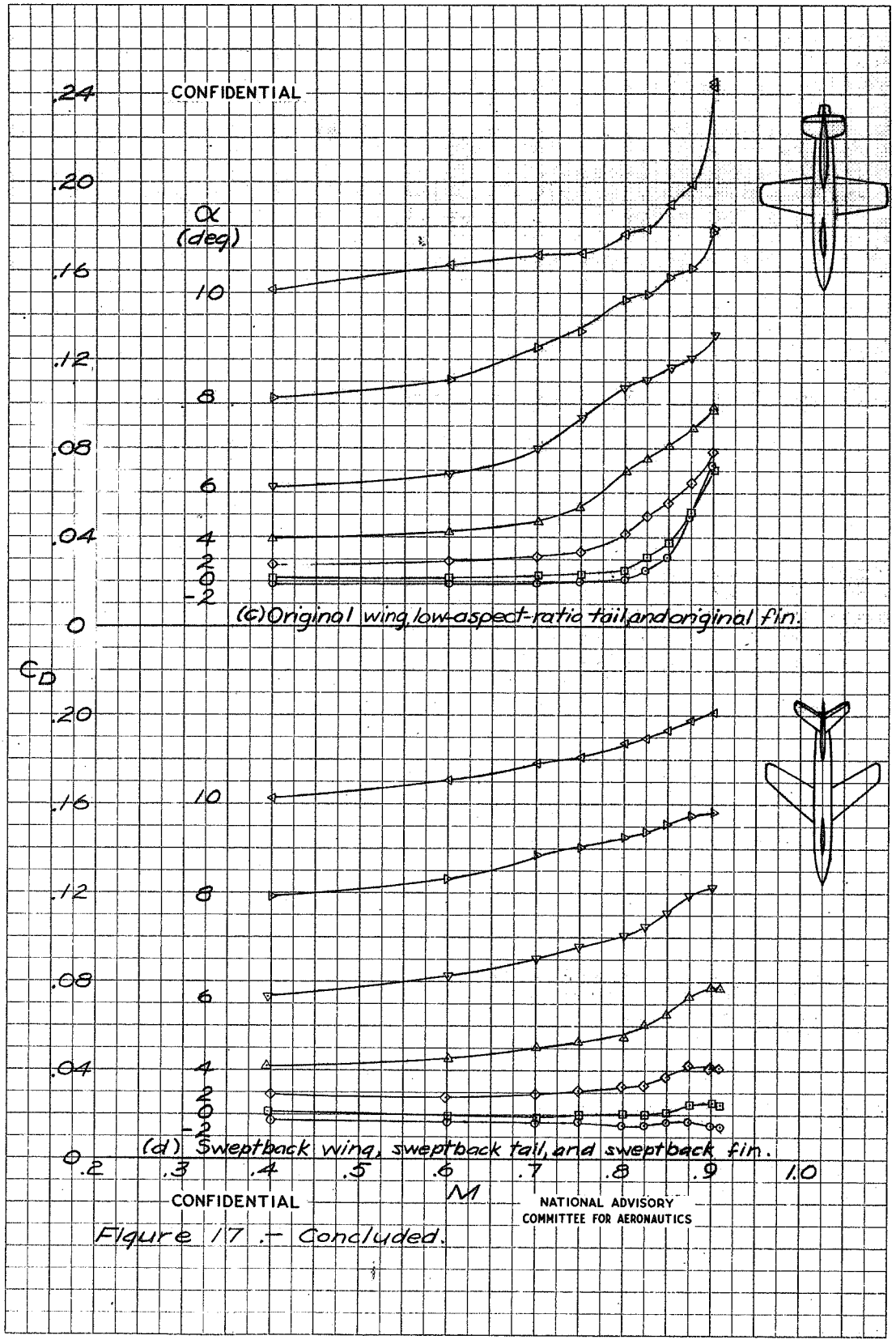

Figure 17.- Concluded.

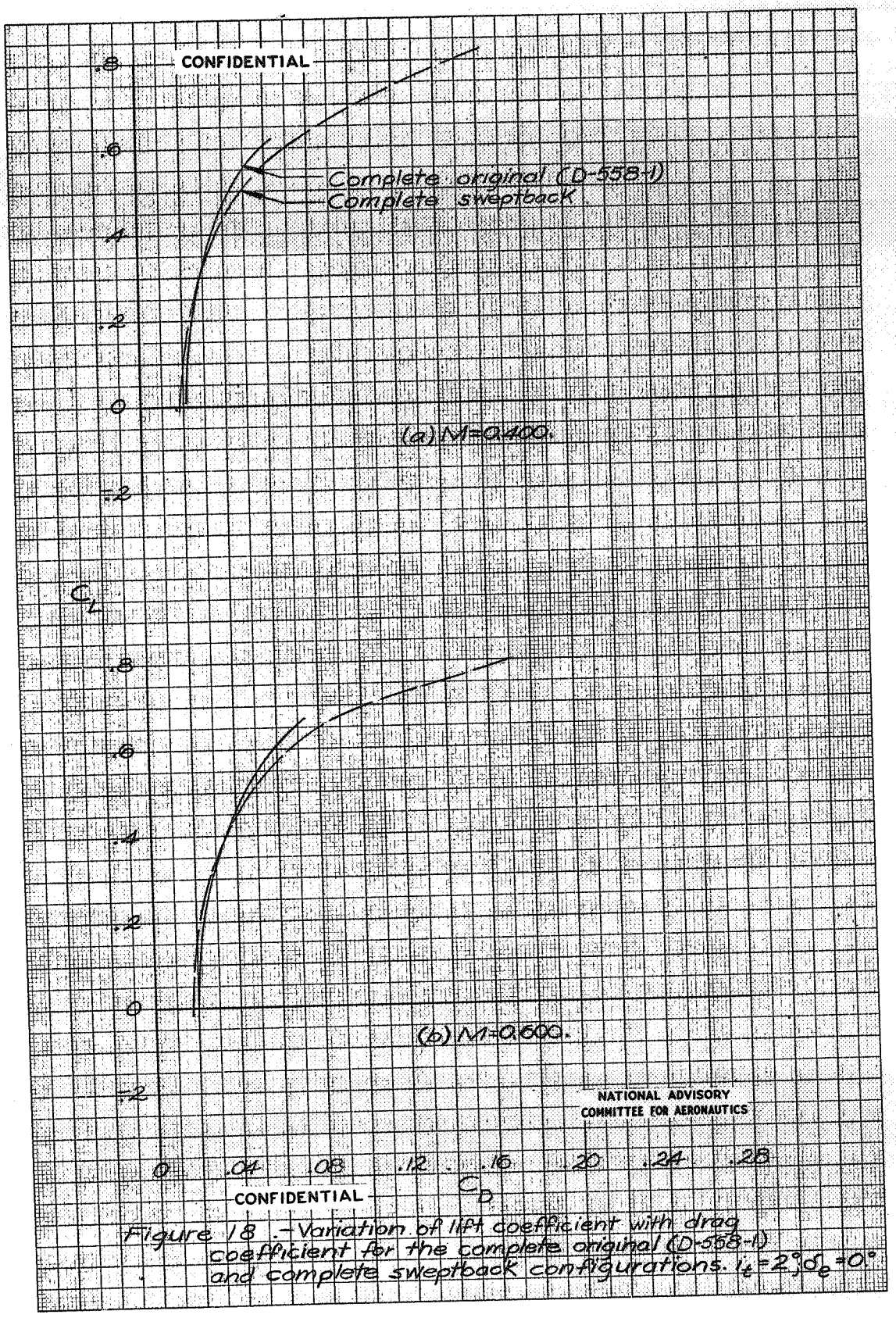

Figure 18.- Variation of lift coefficient with drag coefficient for the complete original (D-558-1) and complete swptback configurations. $i_t = 2°, \delta_e = 0°$.

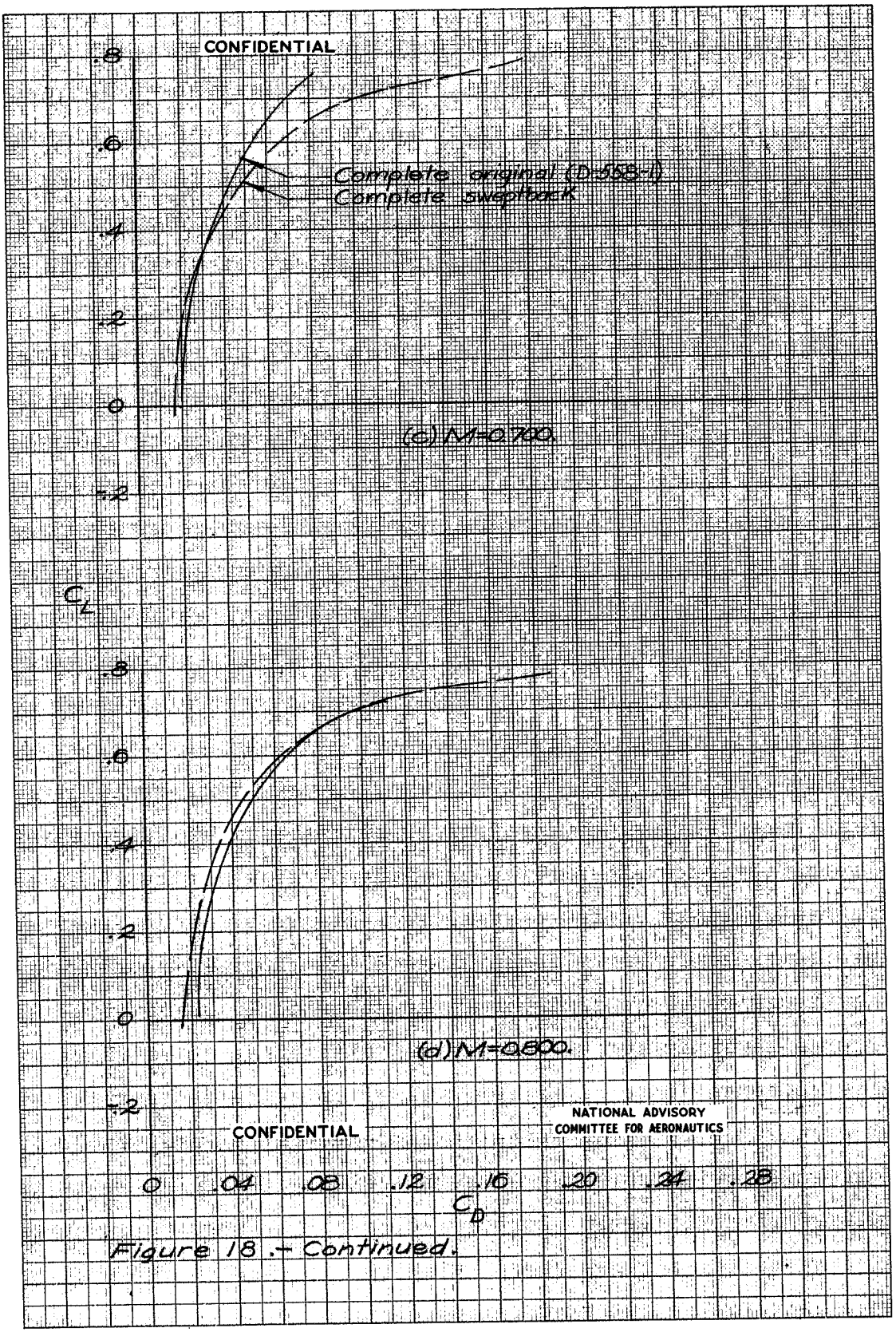

Figure 18.- Continued.

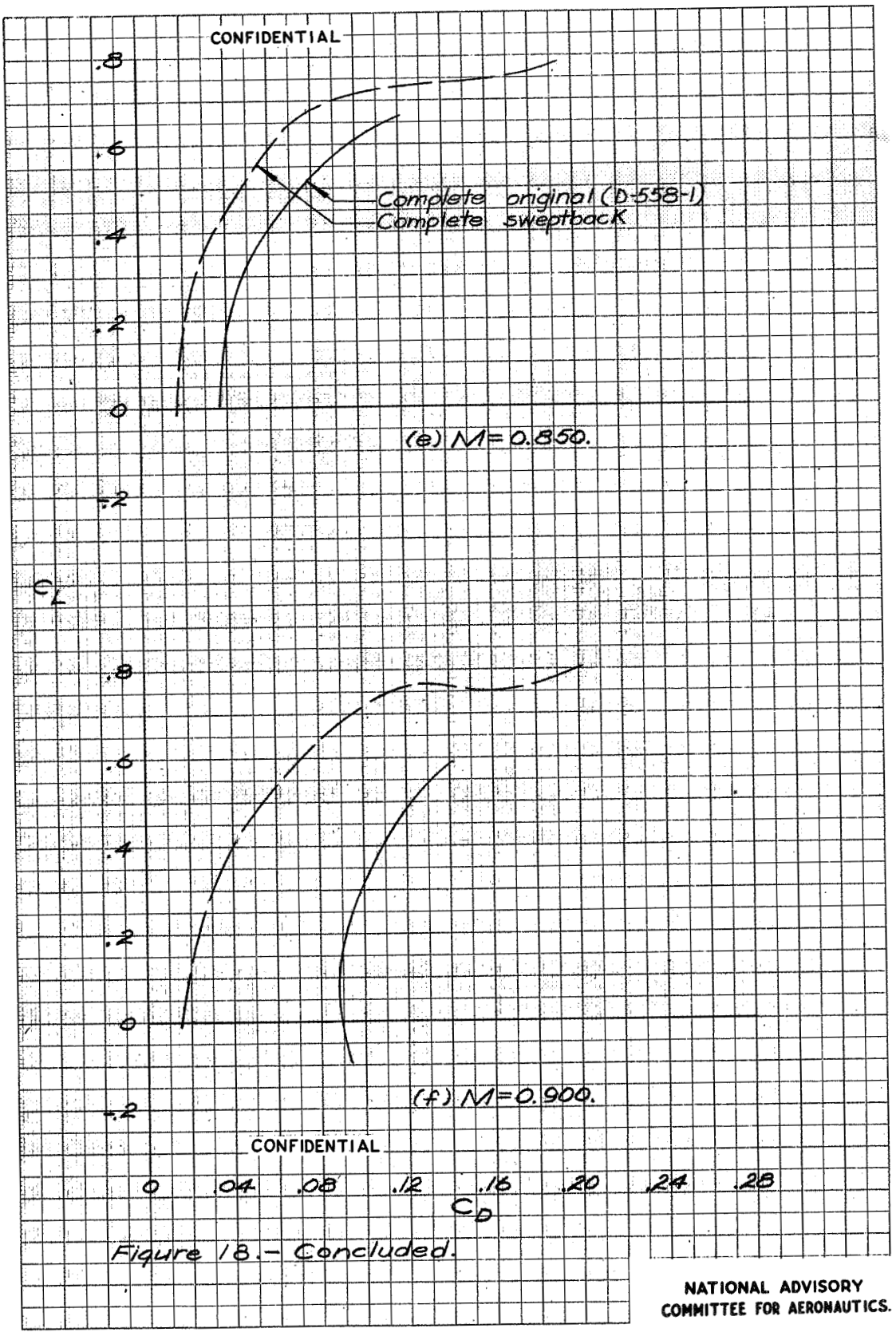

Figure 18.- Concluded.

NATIONAL ADVISORY
COMMITTEE FOR AERONAUTICS.

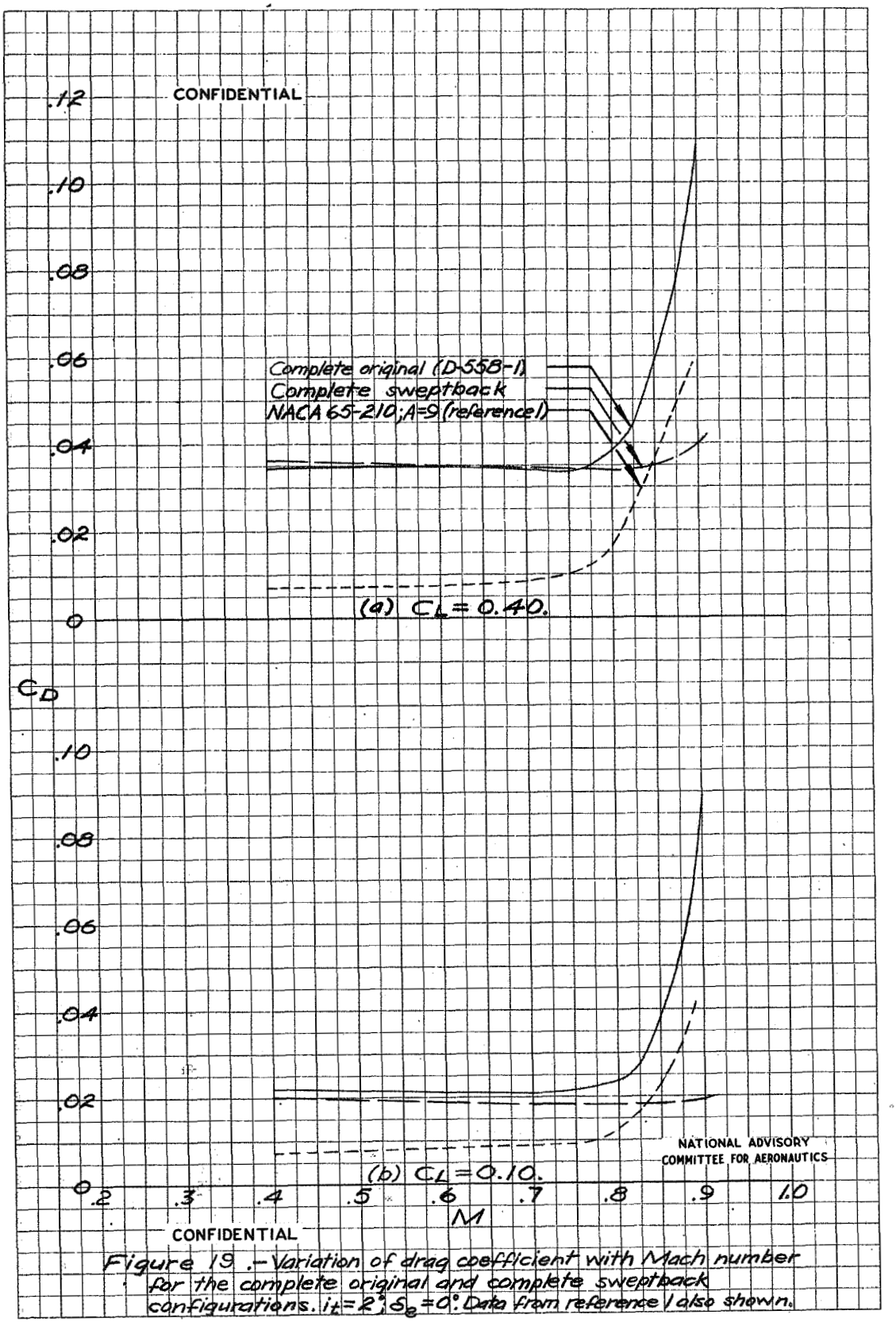

Figure 19.- Variation of drag coefficient with Mach number for the complete original and complete sweptback configurations. $i_t = 2°$; $\delta_e = 0°$. Data from reference 1 also shown.

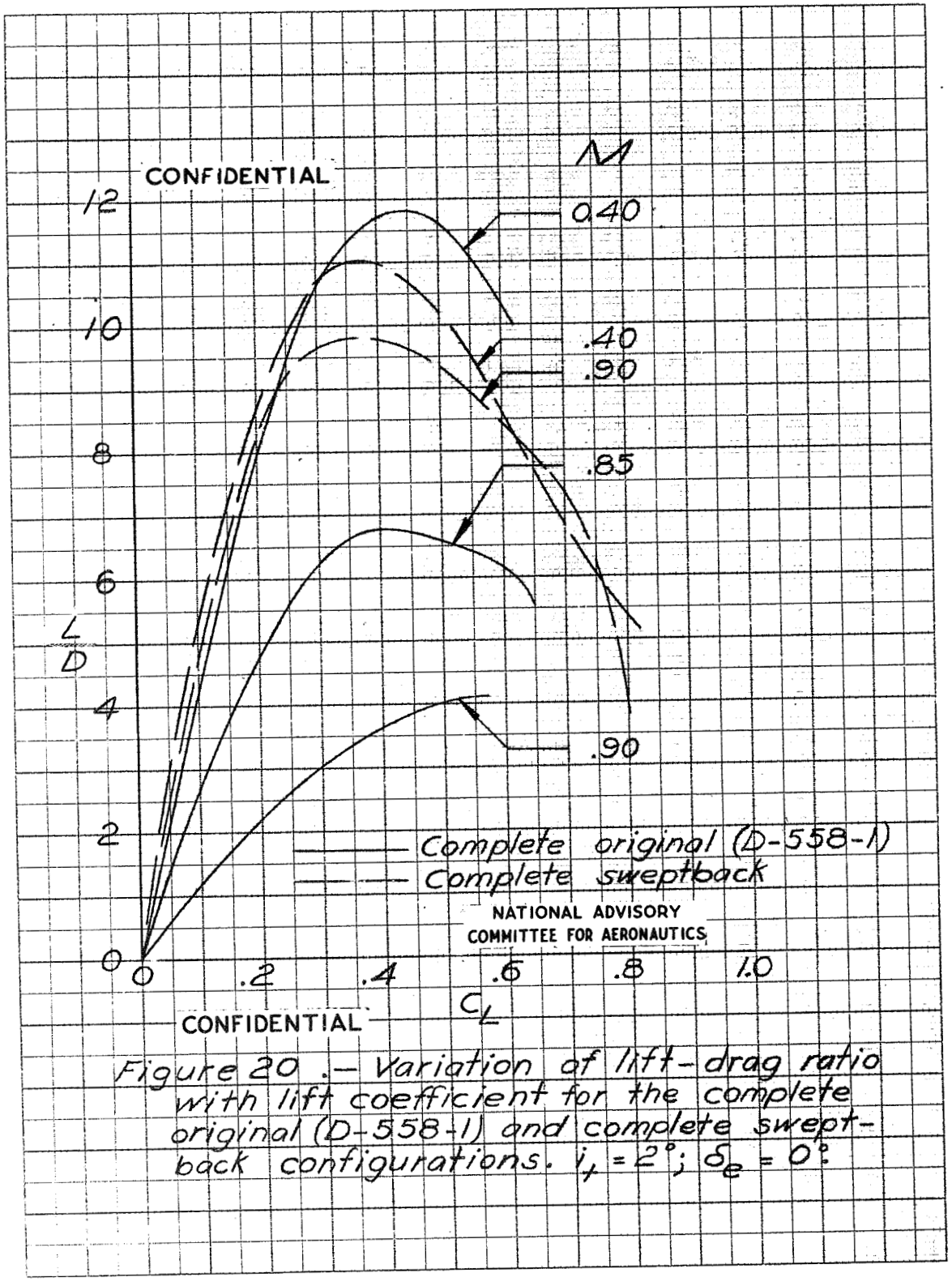

Figure 20 .- Variation of lift-drag ratio with lift coefficient for the complete original (D-558-1) and complete swept-back configurations. $i_t = 2°$; $\delta_e = 0°$.

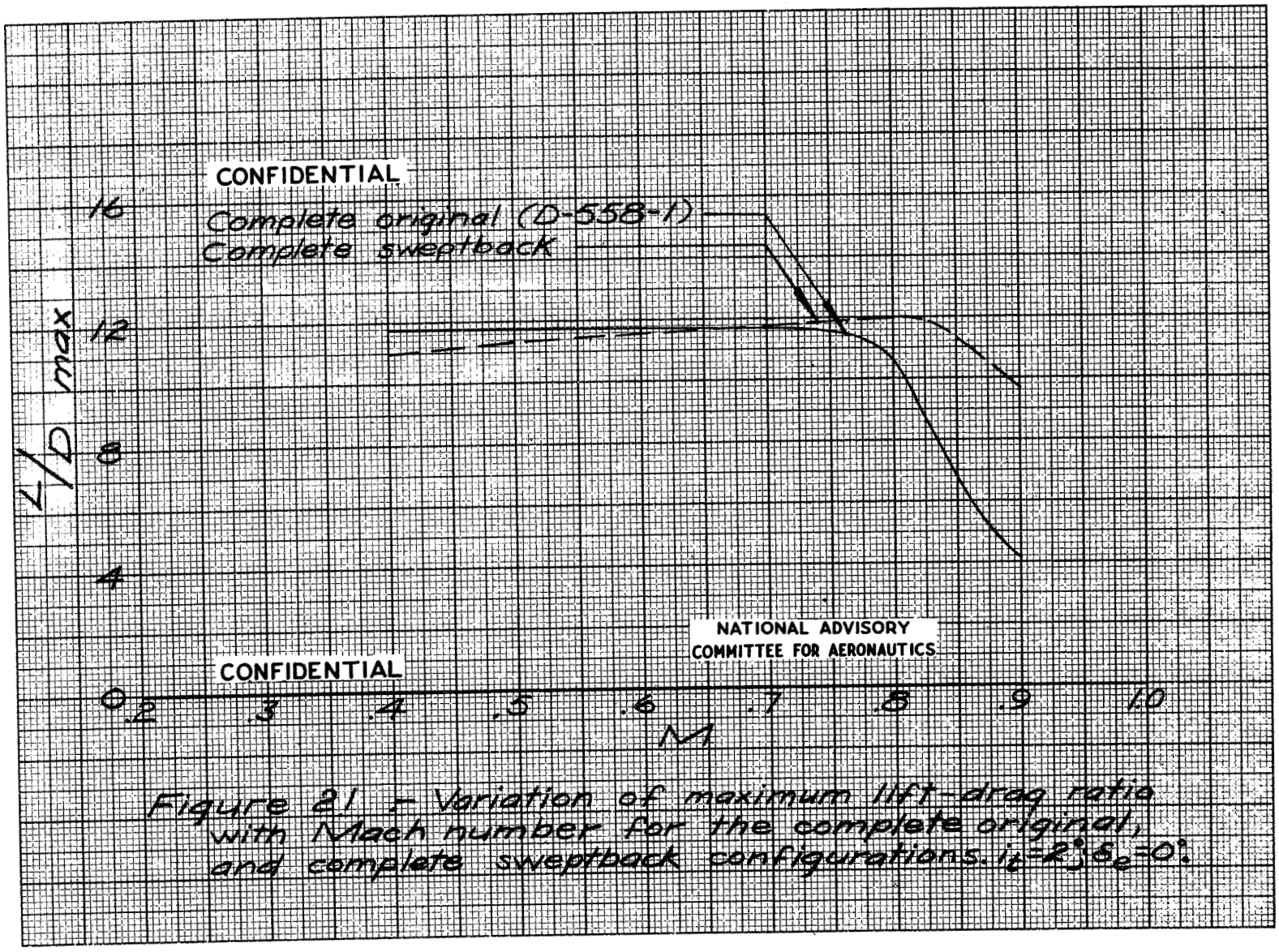

Figure 21.- Variation of maximum lift-drag ratio with Mach number for the complete original and complete sweptback configurations. $i_t = 2°$; $\delta_e = 0°$.